NF-κB signaling drives Th17-mediated lacrimal gland injury and tear dysfunction in a murine model of primary Sjögren's syndrome

JIAJUN XIE[1-4], HUINA ZHANG[1-4], WENYUE SHEN[1-4] and JUAN YE[1-4]

[1]Eye Center of The Second Affiliated Hospital, Zhejiang University School of Medicine, Hangzhou, Zhejiang 310009, P.R. China; [2]Zhejiang Provincial Key Laboratory of Ophthalmology, The Second Affiliated Hospital, Zhejiang University School of Medicine, Hangzhou, Zhejiang 310009, P.R. China; [3]Zhejiang Provincial Clinical Research Center for Eye Diseases, The Second Affiliated Hospital, Zhejiang University School of Medicine, Hangzhou, Zhejiang 310009, P.R. China; [4]Zhejiang Provincial Engineering Institute on Eye Diseases, The Second Affiliated Hospital, Zhejiang University School of Medicine, Hangzhou, Zhejiang 310009, P.R. China

Received September 11, 2025; Accepted April 23, 2026

DOI: 10.3892/mmr.2026.13904

Abstract. Primary Sjögren's syndrome (pSS) is a systemic autoimmune disorder characterized by chronic inflammation of exocrine glands, resulting in lacrimal gland dysfunction, reduced tear secretion and dry eye manifestations. The nuclear factor κB (NF-κB) signaling pathway is a central regulator of inflammatory responses; however, its role in lacrimal gland injury in pSS remains incompletely defined. The present study investigated the contribution of NF-κB signaling to lacrimal gland damage and tear secretion in non-obese diabetic (NOD)/Ltj mice, an established *in vivo* model of pSS. Histopathological alterations were evaluated by hematoxylin and eosin staining. Transcriptomic profiling was performed using mRNA sequencing and validated by western blotting analysis. Pharmacological inhibition of NF-κB was achieved using JSH-23. T helper 17 (Th17) cell differentiation, inflammatory cytokine production, apoptosis and tear secretion were assessed by immunohistochemistry, flow cytometry, enzyme-linked immunosorbent assay, terminal deoxynucleotidyl transferase dUTP nick end labeling staining and the phenol red thread test. NF-κB signaling was markedly activated in the lacrimal glands of NOD/Ltj mice. Inhibition of NF-κB reduced Th17 cell differentiation, decreased proinflammatory cytokine expression, attenuated apoptosis, restored tear secretion and partially normalized the expression levels of differentially expressed genes, including *CARD14* and *CCL19* transcripts and their corresponding proteins, CARD14 and CCL19. These findings indicated that NF-κB signaling contributes to Th17-mediated lacrimal gland injury in pSS and suggested that pharmacological targeting of this pathway may represent a potential therapeutic strategy for pSS-associated dry eye.

Correspondence to: Professor Juan Ye, Eye Center of The Second Affiliated Hospital, Zhejiang University School of Medicine, 88 Jiefang Road, Hangzhou, Zhejiang 310009, P.R. China
E-mail: yejuan@zju.edu.cn

Abbreviations: pSS, primary Sjögren's syndrome; NF-κB, nuclear factor κB; Th17, T helper 17; IL-17A, interleukin-17A; IFN-γ, interferon-γ; TNF-α, tumor necrosis factor-α; IKK, inhibitor of κB kinase; IκBα, inhibitor of κB α; PBMCs, peripheral blood mononuclear cells; DEGs, differentially expressed genes; GO, Gene Ontology; KEGG, Kyoto Encyclopedia of Genes and Genomes; RT-qPCR, reverse transcription-quantitative polymerase chain reaction; ELISA, enzyme-linked immunosorbent assay; TUNEL, terminal deoxynucleotidyl transferase dUTP nick end labeling; IF, immunofluorescence; IHC, immunohistochemistry; SD, standard deviation

Key words: pSS, NF-κB, lacrimal gland, tear production, Th17 cell differentiation

Introduction

Primary Sjögren's syndrome (pSS) is a systemic autoimmune disorder characterized by chronic progressive inflammation, lymphocytic infiltration, exocrine gland destruction and production of disease-specific autoantibodies (1). It has been reported that 70-98% of patients with pSS develop clinically notable dry eye disease globally (2). In the absence of effective intervention, persistent ocular surface inflammation may progress to severe epithelial damage and irreversible visual impairment, markedly compromising quality of life of patients. Progressive lacrimal gland destruction represents a central pathogenic event in pSS-associated aqueous-deficient dry eye (3). Therefore, elucidating the molecular mechanisms underlying lacrimal gland injury is key to developing targeted therapeutic strategies for severe and treatment-refractory disease.

Increasing evidence indicates that a sustained inflammatory microenvironment is a principal driver of target organ damage in pSS. Immune dysregulation, including the type I interferon (IFN) signature (4) and activation of toll-like receptors, promotes the production of proinflammatory cytokines (5). Among these mediators, interleukin

(IL)-17 is consistently elevated and contributes to tissue inflammation through amplification of downstream inflammatory cascades, partly via activation of nuclear factor κB (NF-κB) signaling. Furthermore, aberrant expression of costimulatory molecules, including members of the B7 family (6,7), and activation of the NLR family pyrin domain containing 3 inflammasome (8) further exacerbate immune cell infiltration and glandular injury. Although these immunopathological networks have been extensively investigated in salivary glands (9,10), the specific signaling mechanisms governing lacrimal gland damage remain incompletely defined. Current evidence regarding the lacrimal gland microenvironment indicates that stressed epithelial cells release specific chemokines to recruit dendritic cells and macrophages. Specifically, the secretion of C-X-C motif chemokine ligand 10 drives the recruitment of T helper (Th)1 cells, while the release of CCL20 and CCL19 facilitates the homing of dendritic cells and Th17 subsets. This process initiates the marked infiltration and homing of autoreactive T lymphocytes, predominantly the Th1 and Th17 subsets. The subsequent local accumulation of these immune cells leads to a robust release of proinflammatory cytokines, including IFN-γ and IL-17, which directly drive lacrimal gland destruction (11,12). Recent studies have highlighted potential therapeutic strategies for pSS-related dry eye, such as restoring aquaporin 5 function (13) and suppressing T-cell activation via cyclosporine A (14). However, the molecular mechanisms and specific inflammatory cascades directly driving lacrimal gland pathogenesis remain incompletely elucidated, necessitating further mechanistic investigation in future research.

The non-obese diabetic (NOD)/Ltj mouse is a well-established experimental model of pSS that recapitulates autoantibody production, lymphocytic infiltration and impaired exocrine gland secretion (15-17). Compared with non-autoimmune wild-type control mice, the genetic background of this specific strain is characterized by multiple distinct susceptibility loci and a unique major histocompatibility complex (MHC) class II haplotype. Specifically, the NOD/Ltj strain carries the *H2g7* haplotype, which is characterized by structural alterations in the I-Aβ chain and defective expression of the *Ea* gene, resulting in the absence of functional I-E molecules. In addition to MHC-related features, the NOD/Ltj strain harbors multiple susceptibility loci outside the MHC region, including variants in the *IL2* gene associated with reduced IL-2 production, as well as functional polymorphisms in *CTLA4*. This polygenic genotype fundamentally impairs central and peripheral immune tolerance. Therefore, autoreactive lymphocytes escape deletion and undergo spontaneous activation directly driving the autoimmune exocrinopathy. The present study aimed to delineate the molecular pathways contributing to lacrimal gland injury in pSS-associated dry eye. Specifically, the present study examined the contribution of NF-κB-mediated Th17 responses to local inflammation and tissue damage. Lastly, the present study evaluated whether pharmacological inhibition of NF-κB using JSH-23 could attenuate inflammatory cytokine production, reduce apoptosis and restore tear secretion, thereby establishing a mechanistic association between NF-κB activation and lacrimal gland dysfunction in pSS.

Materials and methods

Animal experiments. To investigate the role of NF-κB signaling in lacrimal gland injury, 20 male NOD/Ltj mice (12 weeks old, weighing 24-28 g) were obtained from Beijing Huafukang Biotechnology Co., Ltd. [Experimental Animal Production License No. SCXK(Jing)2019-0008] and 16 age-matched male Institute of Cancer Research (ICR) mice (weighing 35-40 g) were obtained from Shanghai SLAC Laboratory Animal Co., Ltd. [Experimental Animal Production License No. SCKK(HU)2022-0004]. Animals were housed under specific pathogen-free conditions at 18-22˚C and 40-60% relative humidity with a 12-h light/dark cycle and *ad libitum* access to standard food and water. Mice were maintained until 20 weeks of age prior to experimental analysis.

The systemic dosage of JSH-23 (MedChemExpress) was set at 3 mg/kg daily based on previously validated pharmacological protocols. This dosage has been reported to effectively inhibit NF-κB activation and its downstream proinflammatory cascades in various murine models. Previous studies have confirmed that this specific dose attenuates inflammatory injury in vital organs, including the lung liver and kidney, without inducing notable systemic toxicity (18,19). Therefore, 3 mg/kg JSH-23 was selected to investigate its mechanistic impact on lacrimal gland injury in the present study. In the NOD/Ltj + JSH-23 treatment group (n=6), mice received the NF-κB inhibitor JSH-23 (3 mg/kg) by oral gavage once daily for 4 weeks. Untreated NOD/Ltj mice and ICR control mice received an equal volume of sterile normal saline by oral gavage at the same frequency to control for handling-related stress. At the end of the treatment period, mice were euthanized by cervical dislocation and lacrimal glands were harvested for subsequent analyses. All procedures were conducted in accordance with the Animal Research: Reporting of *In Vivo* Experiments guidelines (20) and complied with the National Institutes of Health Guide for the Care and Use of Laboratory Animals (21). The experimental protocol was approved by the Animal Care and Welfare Committee of Zhejiang University (approval no. 2022-190; Zhejiang, China).

Tear production measurement. To evaluate lacrimal gland secretory function, tear production was measured every 5 days during the initial assessment, and every 4 days beginning at treatment initiation (20 weeks of age) using the phenol red-impregnated cotton thread test (Tianjin Jingming New Technological Development Co. Ltd.) (14). Measurements were continued until 24 weeks of age. During each assessment, mice were gently restrained without anesthesia to avoid suppression of basal tear secretion. The lower eyelid was carefully retracted and one end of the phenol red cotton thread was placed into the lateral canthus of the conjunctival fornix. After 1 min, the length of the wetted red portion of the thread was measured in millimeters (mm) using a calibrated ruler with 0.5-mm precision. Each eye was tested three times consecutively at the same time of day to minimize diurnal variation. All measurements were performed independently by two investigators blinded to group allocation. The final tear secretion value for each eye was calculated as the mean of the measurements obtained by the two observers.

Histopathological evaluation and immunohistochemistry (IHC). To evaluate histopathological alterations and determine *in situ* expression levels of target proteins and immune cell infiltration in lacrimal glands, hematoxylin and eosin (H&E) staining and IHC were performed. Lacrimal gland tissues were fixed in 4% paraformaldehyde (PFA) for 24 h at room temperature, embedded in paraffin and sectioned (thickness, 4 μm). Paraffin sections were deparaffinized and rehydrated through graded ethanol solutions (100% ethanol, two changes, 3 min each; 95% ethanol, 2 min; 70% ethanol, 2 min), followed by rinsing in distilled water.

For H&E staining, sections were stained with hematoxylin for 5 min and counterstained with eosin for 2 min at room temperature to visualize the overall tissue structure and cell morphology. Stained sections were visualized and images were captured using a light microscope (TS100; Nikon Corporation).

For IHC analysis, lacrimal gland tissues were fixed in 4% PFA for 24 h at room temperature and sectioned at a thickness of 4 μm. Antigen retrieval was performed in citrate buffer (pH, 6.0) at 95-100˚C for 15 min, followed by washing with PBS. Endogenous peroxidase activity was blocked with 3% hydrogen peroxide at room temperature for 15 min. Sections were then blocked with 5% bovine serum albumin (BSA) containing 0.3% Triton X-100 (for permeabilization) for 30 min at room temperature and incubated overnight at 4˚C with the following primary antibodies: Anti-CARD14 (cat. no. A16569; 1:50; ABclonal Biotech Co., Ltd.), anti-CCL19 (cat. no. PA5-109488; 1:50; Invitrogen; Thermo Fisher Scientific, Inc.), anti-CD4 (cat. no. MA1-146; 1:50; Invitrogen; Thermo Fisher Scientific, Inc.) and anti-IL-17A (cat. no. sc-374218; 1:50; Santa Cruz Biotechnology, Inc.). After washing with phosphate-buffered saline (PBS), sections were incubated with horseradish peroxidase-conjugated secondary antibody (cat. no. 31460; 1:500; Invitrogen; Thermo Fisher Scientific, Inc.) for 1 h at room temperature. Immunoreactivity was visualized using 3,3'-diaminobenzidine substrate, followed by hematoxylin counterstaining at room temperature for 2 min. Sections were dehydrated, cleared and mounted with coverslips. Images were captured using a light microscope (TS100; Nikon Corporation) at x200 magnification. For quantitative analysis, at least 3 randomly selected non-overlapping fields per section were analyzed using ImageJ software (version 1.48v; National Institutes of Health). The mean integrated optical density or positive staining area per field was calculated for each sample.

mRNA sequencing (mRNA-seq) and bioinformatics analysis. To identify transcriptomic alterations associated with lacrimal gland dysfunction, mRNA-seq was performed on lacrimal gland tissues obtained from NOD/Ltj mice (n=3) and ICR mice (n=3). Total RNA was extracted using TRIzol® reagent (cat. no. 15596026; Invitrogen; Thermo Fisher Scientific, Inc.), according to the manufacturer's protocol. RNA concentration and purity were assessed using a NanoDrop™ spectrophotometer (Thermo Fisher Scientific, Inc.) and RNA integrity was evaluated using an Agilent 2100 Bioanalyzer (Agilent Technologies, Inc.). Samples with an RNA integrity number ≥7.0 were used for library preparation. Poly(A) mRNA was enriched using oligo(dT) magnetic beads and fragmented into short segments. Complementary DNA (cDNA) was synthesized using the NEBNext® Ultra™ II RNA Library Prep Kit for Illumina® (cat. no. E7770S; New England BioLabs, Inc.). The concentration of the final libraries was measured using a Qubit 4.0 Fluorometer (Thermo Fisher Scientific, Inc.), and the final library was loaded at a concentration of 1.5 pM. Libraries were amplified by PCR and validated prior to sequencing. Paired-end sequencing [2x150 bp (PE150)] was performed on an Illumina NovaSeq™ 6000 platform (Illumina, Inc.) using the NovaSeq 6000 S4 Reagent Kit (cat. no. 20028312; Illumina, Inc.).

Raw sequencing reads were filtered to remove adapter sequences and low-quality reads prior to downstream analysis. Differential gene expression analysis between groups was performed using the 'DESeq2' package (version 1.46.0; https://bioconductor.org/packages/DESeq2/) in R software. Genes with $|\log_2$ fold change (FC)$|>1$ and an adjusted P-value (false discovery rate) <0.05 were considered significantly differentially expressed. To functionally annotate the identified differentially expressed genes (DEGs), Gene Ontology (GO) and Kyoto Encyclopedia of Genes and Genomes (KEGG) pathway enrichment analysis were conducted using the 'clusterProfiler' package (version 4.14.6; https://bioconductor.org/packages/clusterProfiler/) in R software (R Development Core Team). GO enrichment analysis categorized the DEGs into biological processes, cellular components and molecular functions. KEGG pathway analysis was performed to identify significantly enriched signaling pathways. Pathways containing >2 genes and an adjusted $P<0.05$ was considered to indicate a statistically significant difference. Transcription factor-associated regulatory networks were constructed using weighted correlation network analysis based on the top 2,000 most variable genes to identify key regulatory modules associated with disease phenotype.

The raw mRNA-seq data generated in the present study have been deposited in the National Center for Biotechnology Information (NCBI) Gene Expression Omnibus database (https://www.ncbi.nlm.nih.gov/geo/) under accession number GSE306385.

Reverse transcription-quantitative polymerase chain reaction (RT-qPCR). To validate differential gene expression identified by mRNA-seq, total RNA was extracted from lacrimal gland tissues using the RNeasy Mini Kit (Qiagen GmbH) according to the manufacturer's instructions. cDNA was synthesized using the iScript™ cDNA Synthesis Kit (Bio-Rad Laboratories, Inc.) according to the manufacturer's protocol (25˚C for 5 min, 46˚C for 20 min and 95˚C for 1 min). qPCR was performed using iTaq™ Universal SYBR® Green SuperMix (Bio-Rad Laboratories, Inc.). Target-specific primers were designed using NCBI Primer-Basic Local Alignment Search Tool (BLAST) to span at least one exon-exon junction. Primer sequences are listed in Table I. Thermocycling conditions were as follows: Initial denaturation at 95˚C for 30 sec, followed by 40 cycles of denaturation at 95˚C for 5 sec and annealing/extension at 60˚C for 30 sec. A melting curve analysis (65-95˚C) was performed at the end of each run to confirm amplification specificity. Relative gene expression levels were calculated using the $2^{-\Delta\Delta Cq}$ method (22), with β-actin serving as the internal reference gene. The specific primers for mouse β-actin were designed using

Table I. Primer sequences used for reverse transcription-quantitative PCR (mouse).

Gene	Primer sequences (5'-3')
CARD14	F: CAGCACTTTCAGCGGTCTC
	R: CATCTCGTCCTTCAGTTTCAG
TNFSF14	F: ATTGGTGGACCTCTGTTATGG
	R: CTAACTCCTTCGGGTAGCG
TNFSF13	F: GGTGATGTGGCAACCAGTA
	R: CCTTGTCCTTCCCGAGATA
CCL19	F: CTGCCTCAGATTATCTGCCAT
	R: CTTCCGCATCATTAGCACCC
CCL20	F: GTGGGTTTCACAAGACAGA
	R: CTCTTAGGCTGAGGAGGTT
CCL12	F: CACTTCTATGCCTCCTGCTC
	R: TGGCTGCTTGTGATTCTCC
β-actin	F: CCCAACTTGATGTATGAAGG
	R: TTTGTGTAAGGTAAGGTGTGC

F, forward; R, reverse.

the NCBI Primer-BLAST software based on the reference cDNA sequence (GenBank accession no. NM_007393.5).

Western blotting. To evaluate the activation of the NF-κB signaling pathway and the expression levels of downstream inflammatory mediators at the protein level, lacrimal gland tissues were homogenized and lysed in radioimmunoprecipitation assay buffer (cat. no. 87787; Thermo Fisher Scientific, Inc.) supplemented with protease and phosphatase inhibitor cocktails. Protein concentrations were determined using a bicinchoninic acid protein assay kit (Thermo Fisher Scientific, Inc.). Equal amounts of total protein (30 μg/lane) were separated in 10% gels using sodium dodecyl sulfate-polyacrylamide gel electrophoresis and transferred onto polyvinylidene difluoride membranes (MilliporeSigma). Membranes were blocked with 5% BSA in Tris-buffered saline (TBS) containing 0.1% Tween-20 (TBST) for 1 h at room temperature and incubated overnight at 4˚C with primary antibodies. After washing with TBST, membranes were incubated with the appropriate infrared dye-conjugated secondary antibodies for 1 h at room temperature in the dark. Protein bands were detected using an Odyssey® Infrared Imaging System (LI-COR Biosciences). Band intensities were quantified using ImageJ software (Version 1.48v; National Institutes of Health). Relative protein expression levels were normalized to β-actin.

Primary antibodies against NF-κB p65 (cat. no. 8242T), phosphorylated (p-) NF-κB p65 (cat. no. 3033T), inhibitor of κB kinase (IKK)α (cat. no. 11930T), IKKβ (cat. no. 8943T), p-IKKα/β (cat. no. 2697T), inhibitor of κBα (IκBα; cat. no. 4814T) and p-IκBα (cat. no. 2859T) were purchased from Cell Signaling Technology, Inc., and used at a dilution of 1:1,000. Antibodies against tumor necrosis factor-α (TNF-α; cat. no. 60291-1-1G) was obtained from Proteintech Group, Inc. and used at a dilution of 1:1,000. The β-actin antibody (cat. no. 20536-1-AP; Proteintech Group, Inc.) was used at a dilution of 1:5,000. The secondary antibodies used were IRDye 800CW Goat anti-Rabbit IgG (cat. no. 926-32211; 1:10,000; LI-COR Biosciences) and IRDye 680RD Goat anti-Mouse IgG (cat. no. 926-68070; 1:10,000; LI-COR Biosciences).

Flow cytometry and cell sorting. At the experimental endpoint, peripheral whole blood samples (~0.8 ml per mouse) were collected from the mice in each experimental group (ICR controls, NOD/Ltj and NOD/Ltj + JSH-23) via retro-orbital venous plexus bleeding. No other clinical procedures or experimental manipulations were performed on the mice on the day of sacrifice prior to blood collection. All samples were obtained as the primary procedure under deep anesthesia. Specifically, anesthesia was induced using 3-4% inhaled isoflurane and maintained at 1.5-2% isoflurane. Deep anesthesia was confirmed by the complete loss of the pedal withdrawal reflex and corneal reflex before initiating the blood collection. The blood was immediately collected into tubes containing EDTA. Peripheral blood mononuclear cells (PBMCs) were isolated using density gradient centrifugation with Ficoll-Paque™ PLUS (cat. no. 17-1440-02; GE Healthcare) according to standard protocols. Briefly, the collected whole blood samples were diluted 1:1 with PBS and carefully layered onto lymphocyte separation medium. Samples were centrifuged at 800 x g for 30 min at room temperature. After centrifugation, the mononuclear cell layer was collected, transferred to a 15 ml tubes and washed twice with PBS at 250 x g for 10 min at room temperature. For intracellular cytokine staining, PBMCs were stimulated with Cell Stimulation Cocktail plus protein transport inhibitors (cat. no. 00-4975-93; 1:500; eBioscience; Thermo Fisher Scientific, Inc.) for 6 h at 37˚C in a 5% CO_2 incubator. Cells were filtered through a 30 μm CELLTrics® filter (Sysmex Corporation) and resuspended in staining buffer. Surface staining was performed using CD4 antibody (cat. no. MA1-146; 1:100; Invitrogen; Thermo Fisher Scientific, Inc.) for 30 min at 4˚C in the dark. After washing, the cells were fixed and permeabilized using the Intracellular Fixation & Permeabilization Buffer Set (cat. no. 88-8824-00; eBioscience; Thermo Fisher Scientific, Inc.) for 30 min at room temperature. Subsequently, the cells were incubated with IL-17 antibodies (cat. no. 45-7177-80; 1:100; Invitrogen; Thermo Fisher Scientific, Inc.) were added to the cell suspension, mixed gently by pulse vortex and incubated for 30 min in the dark at 4˚C. After washing, PBMCs were centrifuged at 300 x g for 5 min at 4˚C and resuspended in PBS for analysis and cell sorting.

Flow cytometric analysis and cell sorting were performed using a BD FACSAria™ III cell sorter (BD Biosciences) equipped with a 100 μm nozzle at 20 psi. Compensation was performed using single-stained controls. Dead cells were excluded using 4',6-diamidino-2-phenylindole (DAPI; Thermo Fisher Scientific, Inc.) staining at room temperature for 5 min. Fluorescence signals were detected using the 488 nm laser with a 530/30 nm filter for Alexa Fluor™ 488 (CD4), a 695/40 nm filter for PerCP-Cy5.5 (IL-17A), and the 355 nm laser with a 450/50 nm filter for DAPI. Data were analyzed using FlowJo software (version 10.8.1; FlowJo, LLC; BD Biosciences). Gating was established using isotype controls and fluorescence minus one controls. $CD4^+IL\text{-}17A^+$ cells were

gated within the lymphocyte population based on forward and side scatter characteristics.

Sorted cells were collected into 1.5 ml RNase-free tubes pre-coated with 1% BSA in PBS containing RNasin® Plus RNase inhibitor (1:25 dilution) for downstream analysis.

Enzyme-linked immunosorbent assay (ELISA). To quantitatively assess systemic inflammatory cytokine levels, whole blood samples were collected into sterile tubes without anticoagulant and allowed to clot at room temperature for 20 min. Samples were centrifuged at 1,000 x g for 20 min at 4˚C and the serum supernatants were carefully collected and stored at -80˚C until analysis. Serum cytokine concentrations were measured using commercial ELISA kits (Jiangsu Meimian Industrial Co., Ltd.), according to the manufacturer's instructions. The following kits were used: IFN-γ (cat. no. MM-0182M1), TNF-α (cat. no. MM-0132M1), IL-17A (cat. no. MM-0759M1) and IL-6 (cat. no. MM-0163M1). Briefly, serum samples and standards were added to antibody-coated 96-well microplates and incubated for 30 min at 37˚C. After washing to remove unbound proteins enzyme-conjugated detection antibodies were added and incubated for 30 min at 37˚C. Following substrate addition, color development was conducted for 15 min at 37˚C and terminated using stop solution and absorbance was measured at 450 nm using a microplate reader. Cytokine concentrations were calculated from standard curves generated using recombinant standards provided in the kits. All samples were analyzed in duplicate and mean values were used for statistical analysis.

TUNEL staining. Apoptosis in lacrimal gland tissues was assessed using a terminal deoxynucleotidyl transferase dUTP nick end labeling (TUNEL) assay. Tissues were fixed in 4% PFA for 24 h at room temperature. Paraffin-embedded tissue sections (4-μm thickness) were deparaffinized, rehydrated and permeabilized with 0.1% Triton X-100 for 5 min at room temperature. Sections were blocked with 5% BSA for 30 min at room temperature and washed with PBS. TUNEL staining was performed using a commercial kit (cat. no. RC-01; http://www.recordbio.com; Shanghai Recordbio Biological Technology Co., Ltd.) according to the manufacturer's instructions. Sections were incubated with the TUNEL reaction mixture for 1 h and counterstained with DAPI (1 μg/ml; 5 min at room temperature). Sections were then mounted using antifade mounting medium (cat. no. S2100; Beijing Solarbio Science & Technology Co., Ltd.).

Images were captured using a fluorescence microscope (TS100-F; Nikon Corporation). Apoptosis was quantified by calculating the percentage of TUNEL$^+$ cells compared with the total number of DAPI-stained nuclei. At least 3 randomly selected non-overlapping fields per section were analyzed using ImageJ software (Version 1.48v; National Institutes of Health).

Immunofluorescence (IF) staining. To evaluate immune cell infiltration and spatial co-localization in lacrimal gland tissues, paraffin sections (thickness, 4 μm) were fixed in 4% PFA for 10 min at room temperature, permeabilized with 0.1% Triton X-100 and blocked with 5% BSA for 30 min at room temperature.

Sections were incubated overnight at 4˚C with primary antibodies against CD4 (cat. no. MA1-146; 1:20; Invitrogen; Thermo Fisher Scientific, Inc.) and IL-17A (cat. no. sc-374218; 1:50; Santa Cruz Biotechnology, Inc.). After washing, sections were incubated for 45 min at room temperature in the dark with Alexa Fluor™ 488-conjugated secondary antibodies (cat. no. A-21121; 1:500; Invitrogen; Thermo Fisher Scientific, Inc.) or Alexa Fluor™ 594 (cat. no. A-11007; 1:500; Invitrogen; Thermo Fisher Scientific, Inc.). Nuclei were counterstained with DAPI (1 μg/ml) for 5 min at room temperature.

Fluorescent and phase-contrast images were captured using a Zeiss Axiovert 200 inverted microscope equipped with AxioCam MRm digital camera and analyzed using AxioVision software (version 4.9.1; Carl Zeiss AG). Confocal images were acquired using a Leica DM6000 B confocal laser scanning microscope (Leica Microsystems GmbH).

Statistical analysis. All experiments were performed using at least three independent biological replicates unless stated otherwise. Data are presented as mean ± standard deviation (SD). Statistical analyses were conducted using GraphPad Prism (version 8.0; Dotmatics). For comparisons between two independent groups, an unpaired two-tailed Student's t-test was used. For comparisons among three groups, one-way analysis of variance followed by Tukey's multiple comparisons test was performed. $P<0.05$ was considered to indicate a statistically significant difference.

Results

Characterization of dry eye-like manifestations and systemic inflammation in NOD/Ltj mice. Phenol red thread assay demonstrated significantly reduced tear secretion in NOD/Ltj mice compared with ICR controls at all assessed time points (all $P<0.001$), with a mean decrease >2 mm (Fig. 1A). Serum cytokine analysis by ELISA revealed significantly elevated levels of IFN-γ, IL-17A and TNF-α in NOD/Ltj mice compared with ICR mice ($P<0.05$), whereas IL-6 levels did not differ significantly between groups (Fig. 1B). Histopathological examination of lacrimal gland sections stained with H&E demonstrated marked glandular atrophy and prominent lymphocytic infiltration in NOD/Ltj mice compared with ICR controls (Fig. 1C). These findings confirmed the presence of lacrimal gland dysfunction and systemic inflammatory activation in NOD/Ltj mice.

Transcriptomic profiling identifies enrichment of NF-κB signaling and Th17 differentiation pathways in lacrimal glands. To investigate molecular mechanisms associated with reduced tear production in NOD/Ltj mice, mRNA-seq was performed on lacrimal gland tissues. A total of 1,109 DEGs were identified compared with ICR controls, including 874 upregulated and 235 downregulated genes. Differential expression patterns are presented in the heatmap (Fig. 2A) and volcano plot (Fig. 2C). GO enrichment analysis categorized the DEGs into biological processes, cellular components and molecular functions, with significant enrichment in immune and inflammatory response-related categories, specifically including 'cellular response to interferon-β', 'positive regulation of T cell proliferation', 'T cell differentiation' and 'adaptive immune

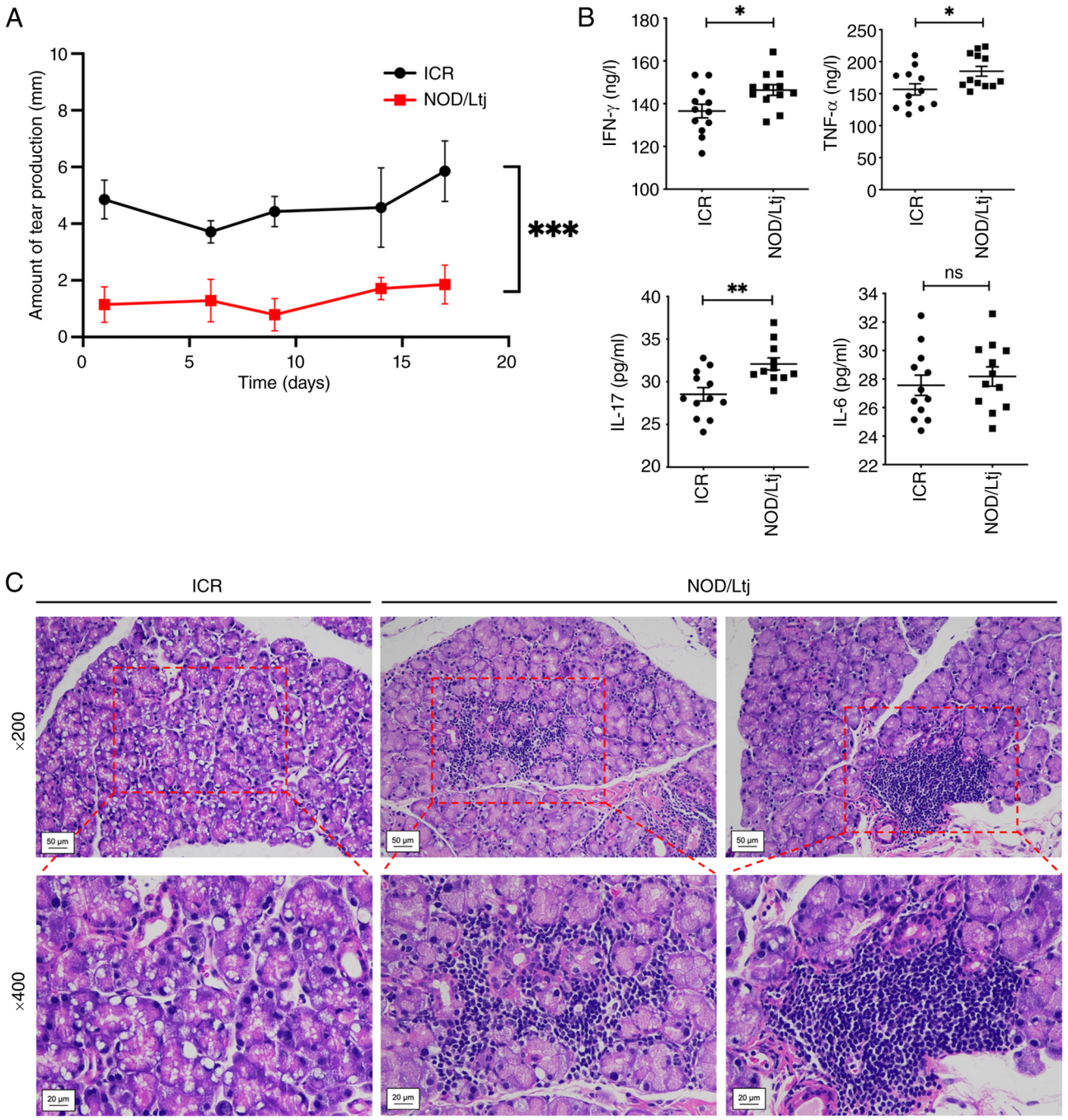

Figure 1. Characterization of lacrimal gland dysfunction and systemic inflammation in NOD/Ltj mice. (A) Tear secretion measured by the phenol red thread test. (B) Serum levels of IFN-γ, IL-17A, TNF-α and IL-6 determined by enzyme-linked immunosorbent assay. (C) Representative hematoxylin and eosin-stained lacrimal gland sections from ICR and NOD/Ltj mice presenting glandular architecture and lymphocytic infiltration (magnification, x200 and x400). Data are presented as mean ± SD (n=12). *P<0.05, **P<0.01 and ***P<0.001; ns vs. ICR control. ns, not significant; ICR, Institute of Cancer Research; IL-17A, interleukin-17A; IFN-γ, interferon-γ; TNF-α, tumor necrosis factor-α; SD, standard deviation; NOD, non-obese diabetic.

response' (Fig. 2B). KEGG pathway analysis demBonstrated significant enrichment of pathways associated with 'NF-κB signaling' and 'Th17 cell differentiation' (Fig. 2D). The NF-κB signaling pathway exhibited an adjusted P-value of 6.71×10^{-12} with a rich factor of 0.29, whereas the Th17 differentiation pathway demonstrated an adjusted P-value of 3.46×10^{-12} with a rich factor of 0.29.

Based on pathway enrichment and differential expression magnitude, six candidate genes were selected for validation: One downregulated gene (*CARD14*: $\log_2$FC, -5.02) and five upregulated genes (*TNFSF14*: $\log_2$FC, 11.64; *TNFSF13*: $\log_2$FC, 0.14; *CCL19*: $\log_2$FC, 3.99; *CCL20*: $\log_2$FC, 4.18; *CCL12*: $\log_2$FC, 2.09). Consistent with the mRNA-seq data, the RT-qPCR analysis confirmed the significant downregulation of *CARD14* (P=0.0412) and upregulation of *CCL19* (P=0.001), consistent with the sequencing results. The expression levels of *CCL12* (P=0.1464) and *CCL20* (P=0.0762), *TNFSF13* (P=0.7954), and *TNFSF14* (P=0.2265) also showed trends consistent with the sequencing data, although these changes did not reach statistical significance (Fig. 3A).

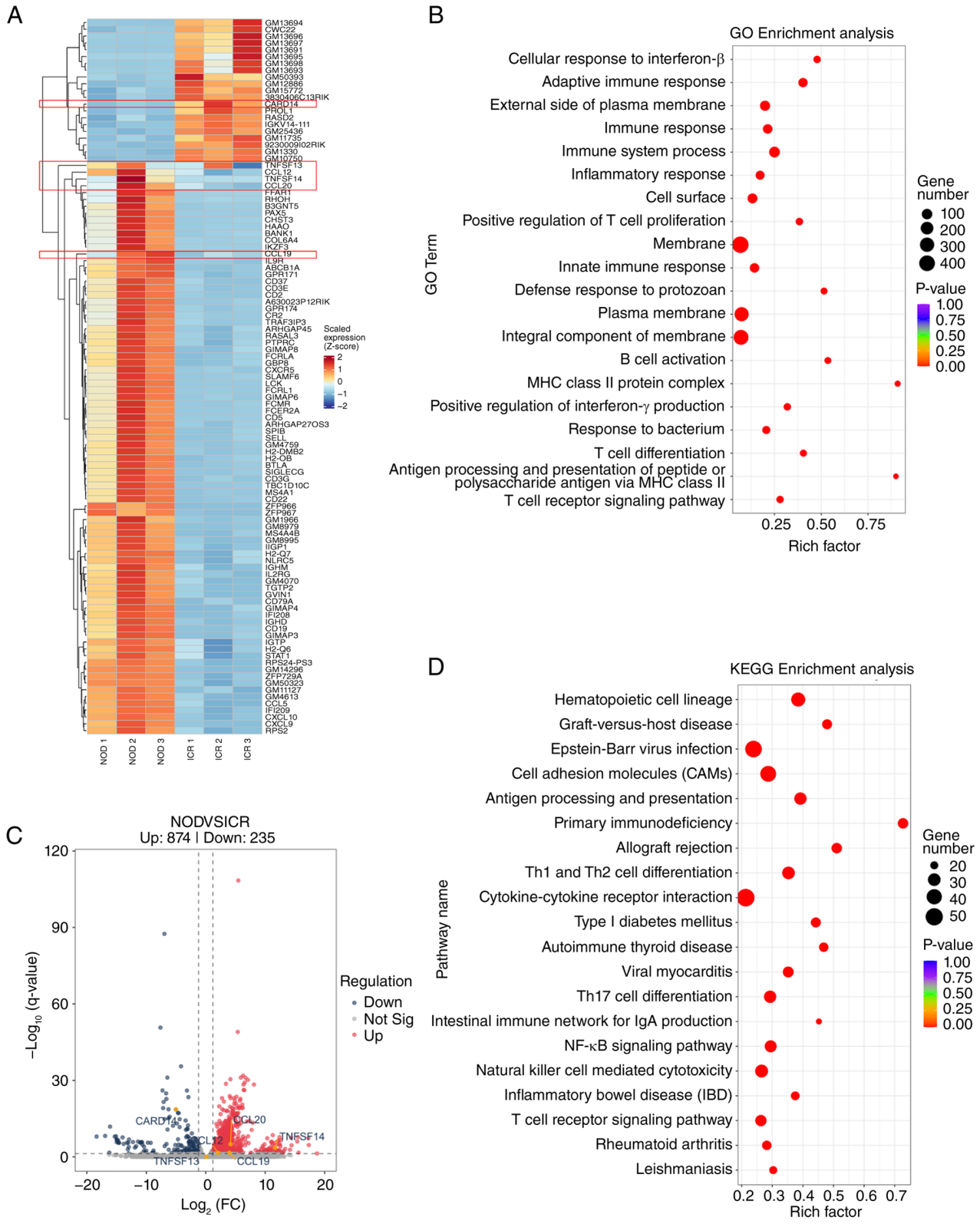

Figure 2. Transcriptomic analysis of lacrimal glands in NOD/Ltj mice. (A) Heatmap presenting DEGs between ICR and NOD/Ltj mice. (B) GO enrichment analysis of DEGs. (C) Volcano plot illustrates the distribution of upregulated and downregulated genes. (D) Kyoto Encyclopedia of Genes and Genomes pathway enrichment analysis. The six genes selected for subsequent reverse transcription-quantitative PCR validation (*CARD14*, *TNFSF14*, *TNFSF13*, *CCL19*, *CCL20* and *CCL12*) are labeled directly in (A) and (C). DEGs were defined as $|\log_2 FC|>1$ and adjusted P-value <0.05. *P<0.05, **P<0.01 and ns. ns, not significant; ICR, Institute of Cancer Research; DEGs, differentially expressed genes; GO, Gene Ontology; FC, fold change; NOD, non-obese diabetic.

To further assess NF-κB pathway activation at the protein level, western blotting analysis was performed. Expression levels of NF-κB pathway components, specifically p-NF-κB (relative to total NF-κB; P=0.0048) and p-IκBα (relative to total IκBα; P=0.0003), were significantly increased in lacrimal glands of NOD/Ltj mice compared with that of ICR controls.

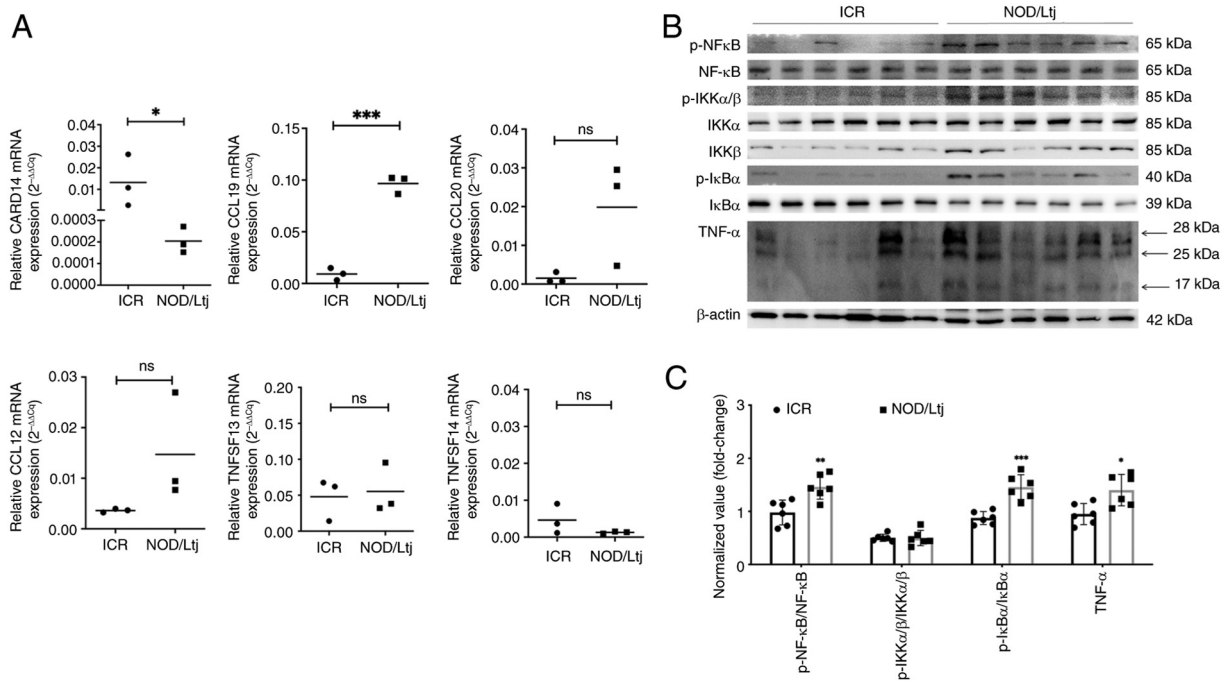

Figure 3. Validation of selected differentially expressed genes and NF-κB pathway activation in lacrimal glands. (A) Relative mRNA expression levels of *CARD14*, *TNFSF14*, *TNFSF13*, *CCL19*, *CCL20* and *CCL12* determined by reverse transcription-quantitative PCR. (B) Representative western blotting images of NF-κB pathway-related proteins and downstream inflammatory mediators. (C) Densitometric quantification of protein expression normalized to β-actin. Data are presented as mean ± SD (n=6). *P<0.05, **P<0.01 and ***P<0.005; ns vs. ICR control. NF-κB, nuclear factor κB; ns, not significant; ICR, Institute of Cancer Research; IKK, inhibitor of κB kinase; IκBα, inhibitor of κB α; TNF-α, tumor necrosis factor-α; SD, standard deviation; p, phosphorylated; NOD, non-obese diabetic.

Furthermore, a significantly elevated level of downstream inflammatory mediator TNF-α was observed (P=0.0112) (Fig. 3B and C). These findings indicated the activation of NF-κB signaling in the lacrimal glands of NOD/Ltj mice.

Pharmacological inhibition of NF-κB attenuates pathway activation and downstream inflammatory mediators in NOD/Ltj mice. To evaluate the functional contribution of NF-κB signaling in pSS-associated lacrimal gland pathology, the NF-κB inhibitor JSH-23 was administered to NOD/Ltj mice. Western blotting analysis demonstrated significantly increased p-NF-κB (P<0.001), -IKKα/β (P=0.0004) and -IκBα (P=0.0002), accompanied by significantly reduced total IκBα expression in NOD/Ltj mice compared with ICR controls (Fig. 4A). Treatment with JSH-23 significantly reduced phosphorylation of NF-κB pathway components (p-NF-κB, P=0.0003; p-IKKα/β, P=0.0009; p-IκBα, P=0.0054 vs. NOD group) and significantly restored IκBα expression (P=0.0023 vs. NOD group) toward levels observed in ICR mice (compared to ICR controls: p-NF-κB, P=0.1525; p-IKKα/β, P=0.0480; p-IκBα, P=0.5786; IκBα, P=0.0878) (Fig. 4A and B). Furthermore, the elevated expression level of downstream inflammatory mediator TNF-α (P=0.0002 vs. ICR group) was significantly reduced following JSH-23 treatment (P=0.0022 vs. NOD group), showing no significant difference compared with the ICR controls (P=0.0586) (Fig. 4A and B). These findings indicated that pharmacological inhibition of NF-κB suppresses pathway activation and downstream inflammatory signaling in NOD/Ltj lacrimal glands.

To assess *in situ* protein expression of selected DEGs, immunohistochemical staining was performed (Fig. 5A). Compared with ICR mice, NOD/Ltj mice exhibited significantly decreased CARD14 protein expression (P=0.0228) and significantly increased CCL19 expression (P=0.0489) in lacrimal gland tissues. Administration of JSH-23 significantly reversed these alterations (CARD14, P=0.0192; CCL19, P=0.0405 vs. NOD group), restoring expression levels similar to those in ICR controls (CARD14, P=0.2349; CCL19, P=0.7356) (Fig. 5B). Therefore, these results demonstrated that NF-κB inhibition modulates CARD14 and CCL19 expression in lacrimal gland tissues of NOD/Ltj mice.

NF-κB inhibition reduces systemic Th17 cell frequency and inflammatory cytokine production in NOD/Ltj mice. To evaluate the effect of NF-κB inhibition on systemic immune responses, PBMCs were analyzed by flow cytometry to quantify $CD4^+$ T cells and $CD4^+IL\text{-}17A^+$ Th17 cells (Fig. 6A and B). The proportion of $CD4^+IL\text{-}17A^+$ cells within the $CD4^+$ T cell population was significantly increased in NOD/Ltj mice compared with ICR controls (P=0.0047), indicating the expansion of Th17 cells. Treatment with JSH-23 significantly reduced the $CD4^+IL\text{-}17A^+/CD4^+$ ratio compared with the untreated NOD/Ltj mice (P=0.0011), restoring levels toward those observed in ICR controls.

Consistent with changes in Th17 cell frequency, ELISA demonstrated significantly elevated serum levels of IFN-γ (P=0.0009), IL-17A (P=0.0002) and TNF-α (P<0.0001) in NOD/Ltj mice compared with ICR controls (Fig. 6C). Administration of JSH-23 significantly reduced the

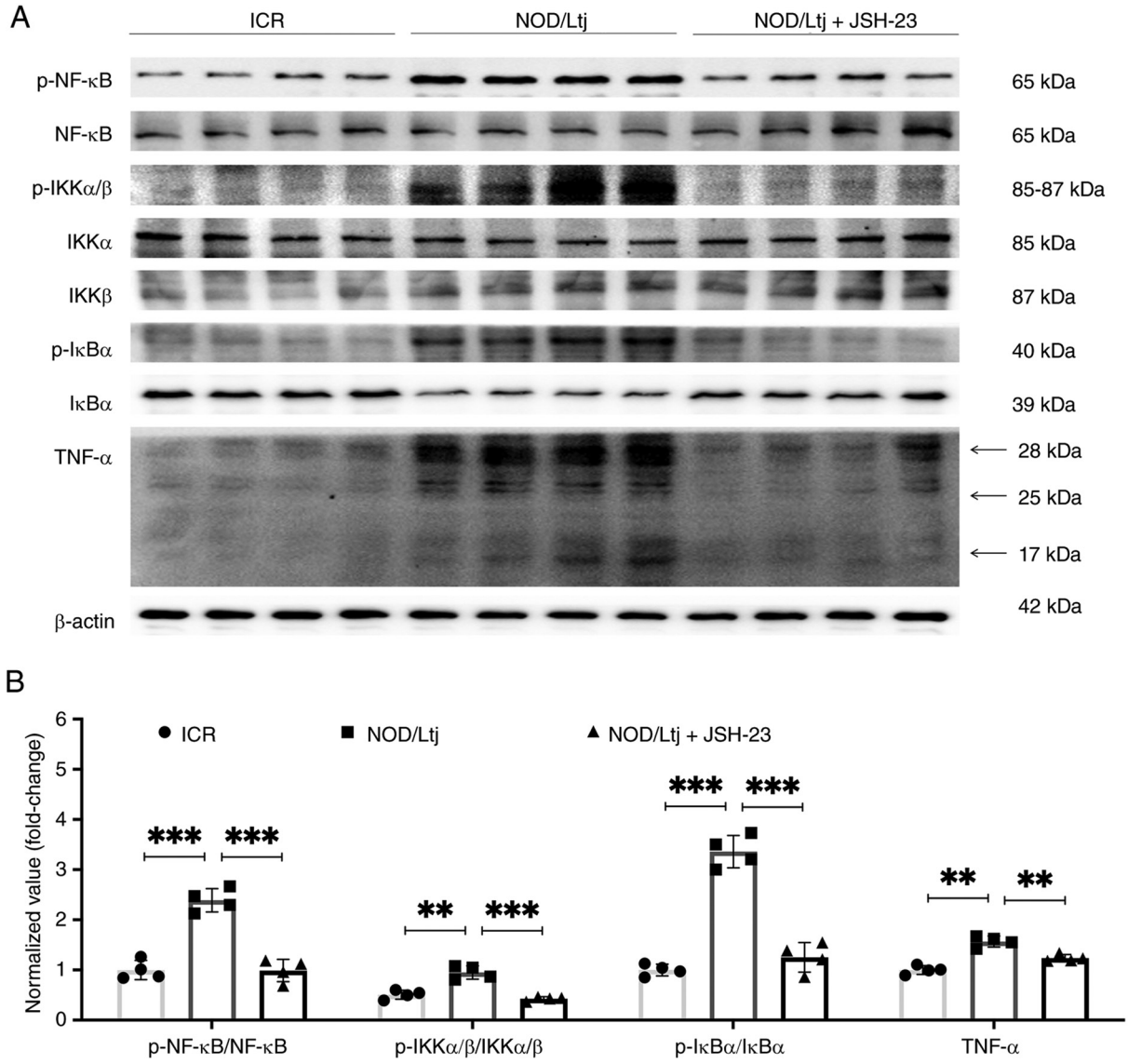

Figure 4. JSH-23 suppresses NF-κB pathway activation in lacrimal glands of NOD/Ltj mice. (A) Representative western blotting images presenting expression levels of NF-κB pathway-related proteins and downstream inflammatory mediators in ICR, NOD/Ltj and NOD/Ltj + JSH-23 groups. (B) Densitometric quantification of protein expression normalized to β-actin. Data are presented as mean ± SD (n=4). **P<0.01 and ***P<0.001 vs. NOD/Ltj group; ns vs. ICR control. NF-κB, nuclear factor κB; ns, not significant; SD, standard deviation; ICR, Institute of Cancer Research; IKK, inhibitor of κB kinase; IκBα, inhibitor of κB α; TNF-α, tumor necrosis factor-α; p, phosphorylated; NOD, non-obese diabetic.

cytokine levels compared with untreated NOD/Ltj mice (IFN-γ, P=0.0151; IL-17A, P=0.0099; and TNF-α, P=0.0019), and restored them to levels with no significant differences compared with the ICR controls (P=0.0590, P=0.0599 and P=0.0502, respectively), indicating suppression of systematic inflammatory cytokine production.

NF-κB inhibition reduces local Th17 cell infiltration in lacrimal glands. To evaluate local immune cell infiltration in lacrimal gland tissues, IHC and IF analyses were performed (Fig. 7). IHC demonstrated significantly increased CD4$^+$ T cell (P=0.0091) and IL-17A expression (P=0.0095) in lacrimal glands of NOD/Ltj mice compared with ICR controls (Fig. 7A and B). Treatment with JSH-23 significantly reduced CD4$^+$ and IL-17A staining intensity (P=0.0190 and P=0.0170 vs. NOD group, respectively), restoring levels toward those observed in the ICR mice. Consistently, IF staining confirmed significantly increased infiltration of CD4$^+$ (P=0.0033) and IL-17A$^+$ (P=0.0434) cells in the lacrimal gland tissues of NOD/Ltj mice, which was significantly attenuated following JSH-23 administration (P=0.0042 and P=0.0302 vs. NOD group, respectively), showing no significant differences compared with the ICR baseline (P=0.9849 and P=0.5101, respectively) (Fig. 7C and D). These findings indicated that inhibition of NF-κB signaling reduces local Th17-associated inflammatory infiltration in lacrimal glands of NOD/Ltj mice.

NF-κB inhibition reduces lacrimal gland apoptosis and partially restores tear secretion. TUNEL staining demonstrated a significantly higher proportion of apoptotic cells in lacrimal gland tissues of NOD/Ltj mice compared with ICR controls (P=0.0476; Fig. 8A and B). Quantitative analysis demonstrated that JSH-23 treatment reduced the percentage of TUNEL$^+$ cells compared with untreated NOD/Ltj mice

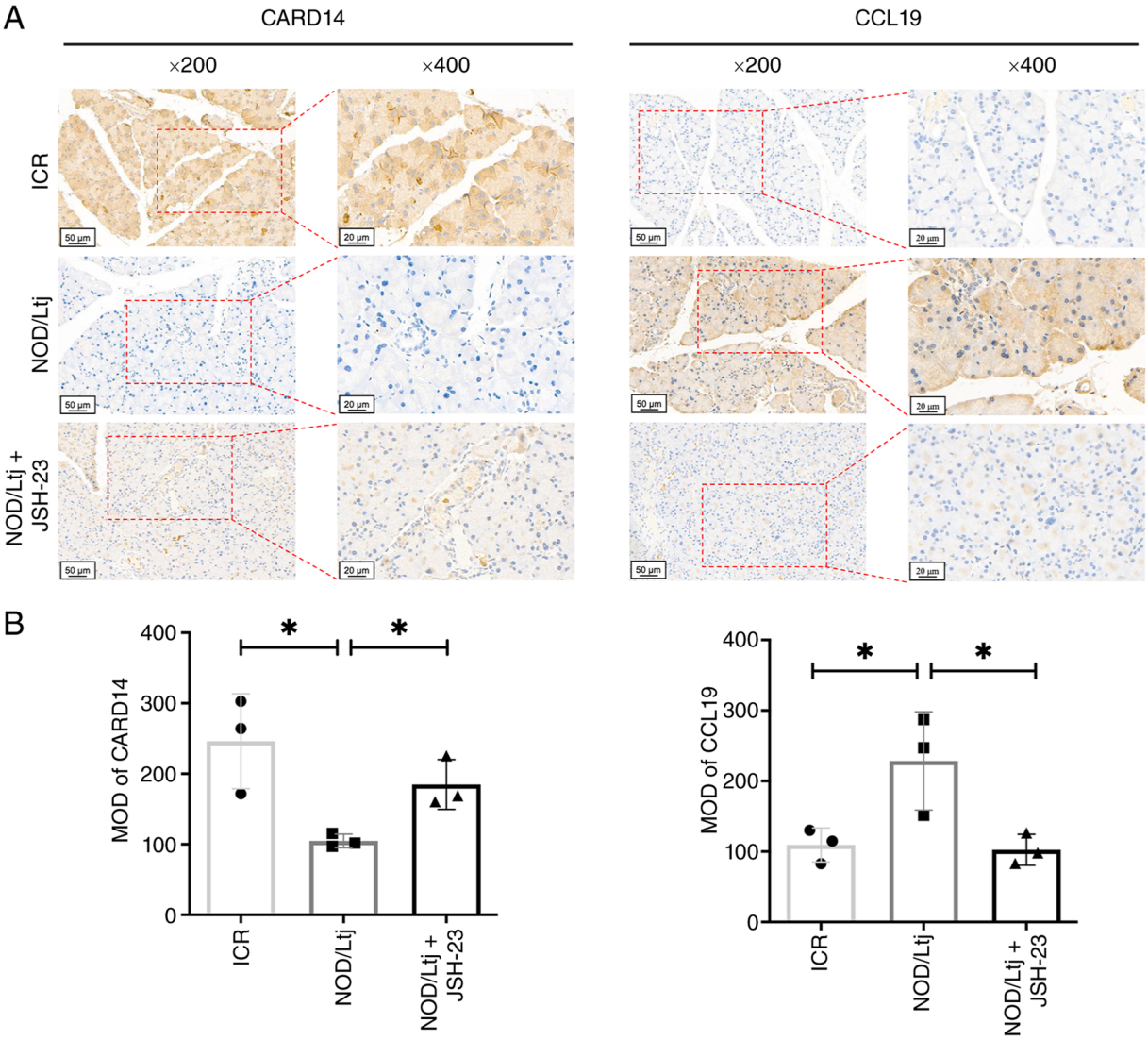

Figure 5. JSH-23 modulates CARD14 and CCL19 expression in lacrimal glands of NOD/Ltj mice. (A) Representative immunohistochemical staining of CARD14 and CCL19 in lacrimal gland sections from ICR, NOD/Ltj and NOD/Ltj + JSH-23 groups (magnification, x200 and x400). (B) Quantitative analysis of CARD14 and CCL19 staining intensity. The y-axis represents MOD. Data are presented as mean ± SD (n=4). *P<0.05 vs. NOD/Ltj group; ns vs. ICR control. ns, not significant; MOD, mean optical density; SD, standard deviation; ICR, Institute of Cancer Research; NOD, non-obese diabetic.

(P=0.0428), restoring apoptosis levels toward those observed in ICR controls (P=0.8763).

To assess the functional impact of NF-κB inhibition on tear secretion, phenol red thread assay was performed. Tear production in NOD/Ltj mice was significantly reduced compared with ICR mice at the final assessment time point (53 days; P=0.0038) (Fig. 8C). Treatment with JSH-23 significantly increased tear production compared with untreated NOD/Ltj mice (P=0.0320), indicating partial restoration of lacrimal gland secretory function.

Discussion

Due to the technical challenges associated with lacrimal gland biopsy in humans, the diagnosis of pSS and studies of target organ injury have largely relied on minor salivary gland biopsy specimens (23-25). Therefore, investigations on lacrimal gland pathology in pSS-related dry eye has predominantly depended on experimental mouse models that effectively bridge this clinical knowledge gap. The NOD/Ltj mouse is extensively used as a spontaneous model of pSS, because it recapitulates key clinical and immunological features of the disease in patients, including reduced tear secretion, lymphocytic infiltration of exocrine glands and elevated systemic inflammatory cytokines (15). Notably, sex-specific differences have been described in this model, with prominent dacryoadenitis observed in men and sialadenitis in women (16). In the present study, male NOD/Ltj mice exhibited marked lacrimal gland dysfunction characterized by reduced tear production, extensive lymphocytic infiltration and germinal center-like structures, accompanied by elevated serum levels of IFN-γ, TNF-α and IL-17A. These findings were consistent with previous studies regarding human pSS immunopathology and confirmed the suitability of this model in investigating the specific mechanisms of lacrimal gland injury in pSS (26-28).

Previous transcriptomic studies in pSS have primarily focused on salivary gland tissue (29,30) and peripheral blood (31-33), with limited analysis of lacrimal gland-specific

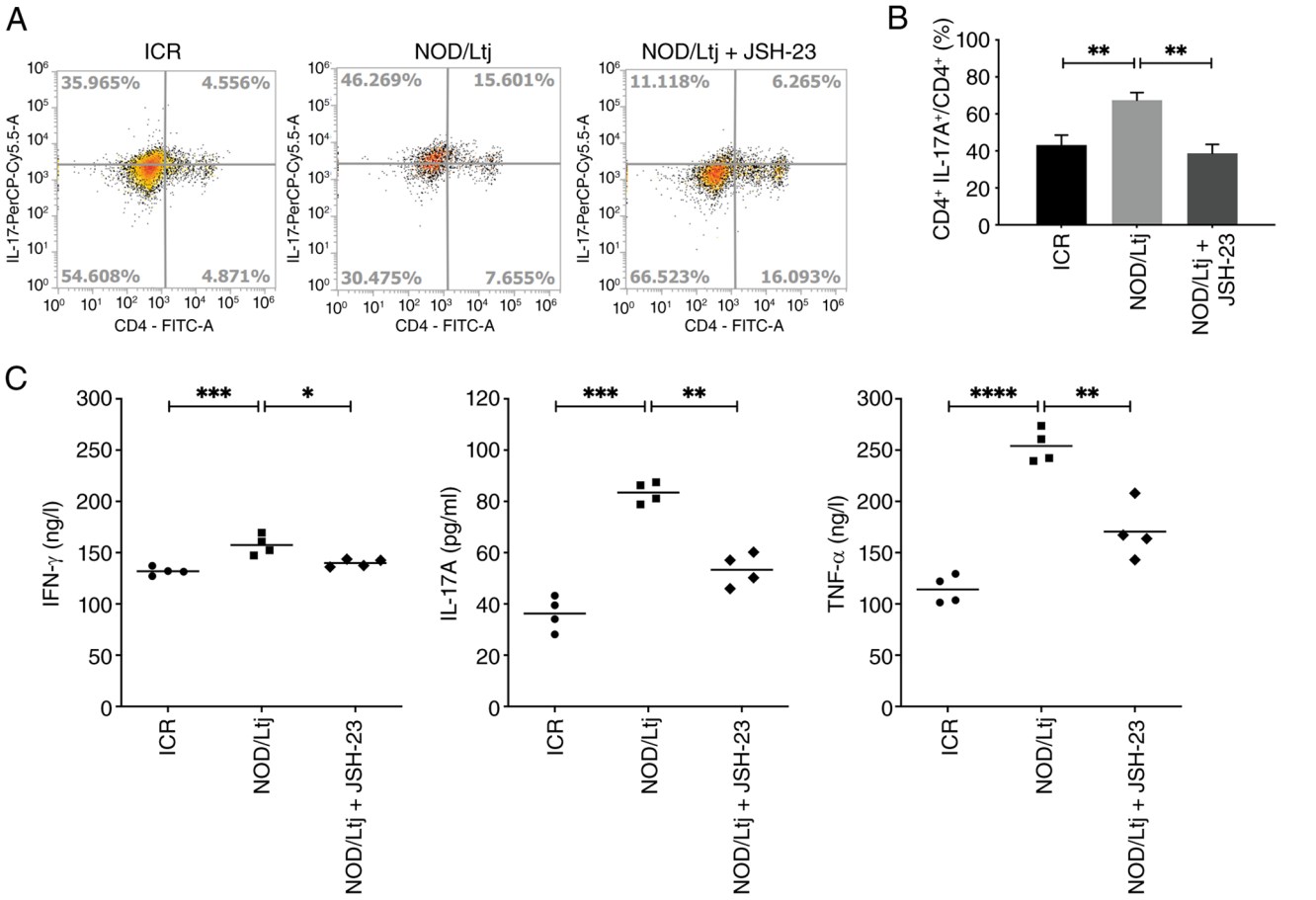

Figure 6. JSH-23 reduces systemic Th17 cell frequency and inflammatory cytokine production in NOD/Ltj mice. (A) Representative flow cytometry plots presenting $CD4^+$ and $CD4^+IL\text{-}17A^+$ cells in peripheral blood mononuclear cells from ICR, NOD/Ltj and NOD/Ltj + JSH-23 groups. (B) Quantitative analysis of the proportion of $CD4^+IL\text{-}17A^+$ cells within the $CD4^+$ T cell population. (C) Serum levels of IFN-γ, IL-17A and TNF-α measured by enzyme-linked immunosorbent assay. Data are presented as mean ± SD (n=6). $^*P<0.05$, $^{**}P<0.01$, $^{***}P<0.001$ and $^{****}P<0.0001$ vs. NOD/Ltj group; ns, not significant vs. ICR control. SD, standard deviation; Th17, T helper 17; NOD, non-obese diabetic; ICR, Institute of Cancer Research; IL-17A, interleukin-17A; IFN-γ, interferon-γ; TNF-α, tumor necrosis factor-α.

molecular alterations (34,35). Although earlier microarray approaches have identified pathways associated with dacryoadenitis in NOD mice (36), a high resolution transcriptomic characterization of the lacrimal gland microenvironment remains to be elucidated. In the present study, the application of high-throughput mRNA-seq allowed for a more sensitive and comprehensive characterization of the lacrimal gland transcriptome. The present study data revealed significant enrichment of immune activation and inflammatory response pathways, with prominent involvement of 'NF-κB signaling' and 'Th17 cell differentiation' pathways. While these pathways are recognized as key drivers of pSS pathogenesis in systemic and salivary gland contexts, the present study findings provide specific transcriptomic evidence of their coordinated dysregulation within the lacrimal gland.

Several key DEGs were selected for validation based on their functional roles in the NF-κB pathway and immune regulation. *CARD14* was selected for its pivotal role as an activator of the NF-κB pathway, mediating inflammatory responses through signaling complex formation (37). *TNFSF14* and *TNFSF13* were included due to their involvement in immune regulation via NF-κB: *TNFSF14* promotes T-cell activation and Th17 responses through NF-κB-dependent pathways (38,39), while *TNFSF13* contributes to B cell hyperactivity (40). Chemokines *CCL19*, *CCL20* and *CCL12* were chosen for their roles in immune cell recruitment and Th17 cell migration. Specifically, *CCL20* facilitates Th17 trafficking via CCR6 (41), *CCL19* regulates T- and dendritic cell migration through CCR7 (42), and CCL12 facilitates monocyte recruitment via CCR2 (43).

Among the DEGs, *CARD14* and *CCL19* were selected for further validation. CARD14 is a scaffold protein predominantly expressed in epithelial cells (44) and known to facilitate NF-κB activation through assembly of signaling complexes (45). While gain-of-function mutations in the CARD14 can disrupt its autoinhibitory conformation and promote aberrant NF-κB activation in inflammatory disorders such as psoriasis (46), the present study findings revealed a distinct expression pattern in the pSS lacrimal gland. Specifically, reduced CARD14 expression was observed in untreated NOD/Ltj lacrimal glands. Due to the predominant epithelial localization of CARD14, its downregulation likely reflects epithelial cell loss secondary to chronic inflammatory injury rather than reduced pathway activity. Following JSH-23 administration, the reduction in glandular apoptosis was accompanied by a marked restoration in CARD14 expression. This restoration suggested that CARD14 levels may serve as a sensitive indicator of epithelial

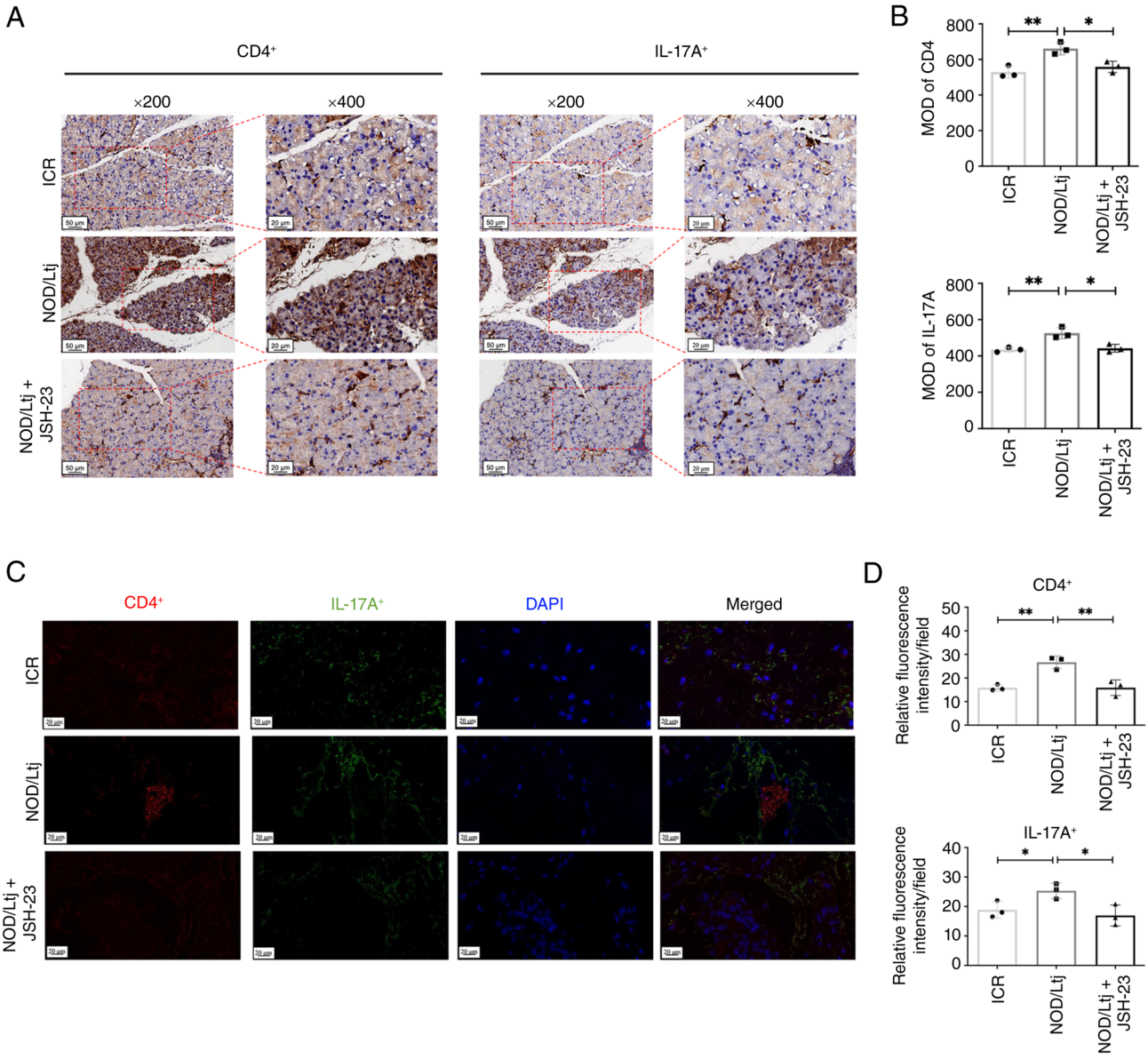

Figure 7. JSH-23 reduces local Th17 cell infiltration in lacrimal glands of NOD/Ltj mice. (A) Representative immunohistochemical staining of $CD4^+$ and $IL\text{-}17A^+$ cells in lacrimal glands (magnification, x200 and x400). (B) Quantitative analysis of $CD4^+$ and $IL\text{-}17A^+$ cell infiltration based on mean optical density (MOD). (C) Representative immunofluorescence staining of $CD4^+$ T cells and IL-17A in lacrimal gland sections from ICR, NOD/Ltj and NOD/Ltj + JSH-23 groups (scale bars, 20 μm). (D) Quantitative analysis of $CD4^+$ and $IL\text{-}17A^+$ fluorescence intensity. Data are presented as mean ± SD (n=4 per group). $^*P<0.05$ and $^{**}P<0.01$ vs. NOD/Ltj group; ns, not significant vs. ICR control. MOD, mean optical density; SD, standard deviation; NOD, non-obese diabetic; ICR, Institute of Cancer Research; Th17, T helper 17; IL-17A, interleukin-17A.

structural integrity. The alignment of CARD14 restoration with the observed decrease in $TUNEL^+$ cells reflects an overall improvement in epithelial cell survival following the attenuation of local inflammation.

By contrast, *CCL19* was markedly upregulated in NOD/Ltj lacrimal glands. CCL19 is a chemokine that actively recruits lymphocytes and contributes to immune cell accumulation in inflamed tissues (47). While the involvement of CCL19 has been reported in the salivary glands of patients with pSS (30), its specific regulation within the lacrimal gland microenvironment remains less characterized. NF-κB has been reported to regulate CCL19 transcription under inflammatory conditions (48,49). The present study findings supported this regulatory relationship in the lacrimal gland, as NF-κB activation was associated with elevated CCL19 expression and increased immune cell infiltration. Pharmacological inhibition of NF-κB significantly reduced CCL19 levels, suggesting that suppression of chemokine-driven immune recruitment represents a key mechanism underlying the anti-inflammatory effects of JSH-23 within the pSS lacrimal gland.

Increasing evidence supports a key role for NF-κB signaling in target organ injury in pSS (50). In salivary glands, NF-κB activation promotes lymphocytic infiltration and pro-inflammatory cytokine production (5,51,52). In the present study, the western blotting analysis demonstrated hyperactivation of the canonical NF-κB pathway in lacrimal glands of NOD/Ltj mice, as evidenced by increased phosphorylation of NF-κB p65, IKKα/β and IκBα. These findings extend previous observations to the lacrimal gland and support a key role for NF-κB mediated inflammatory signaling in glandular

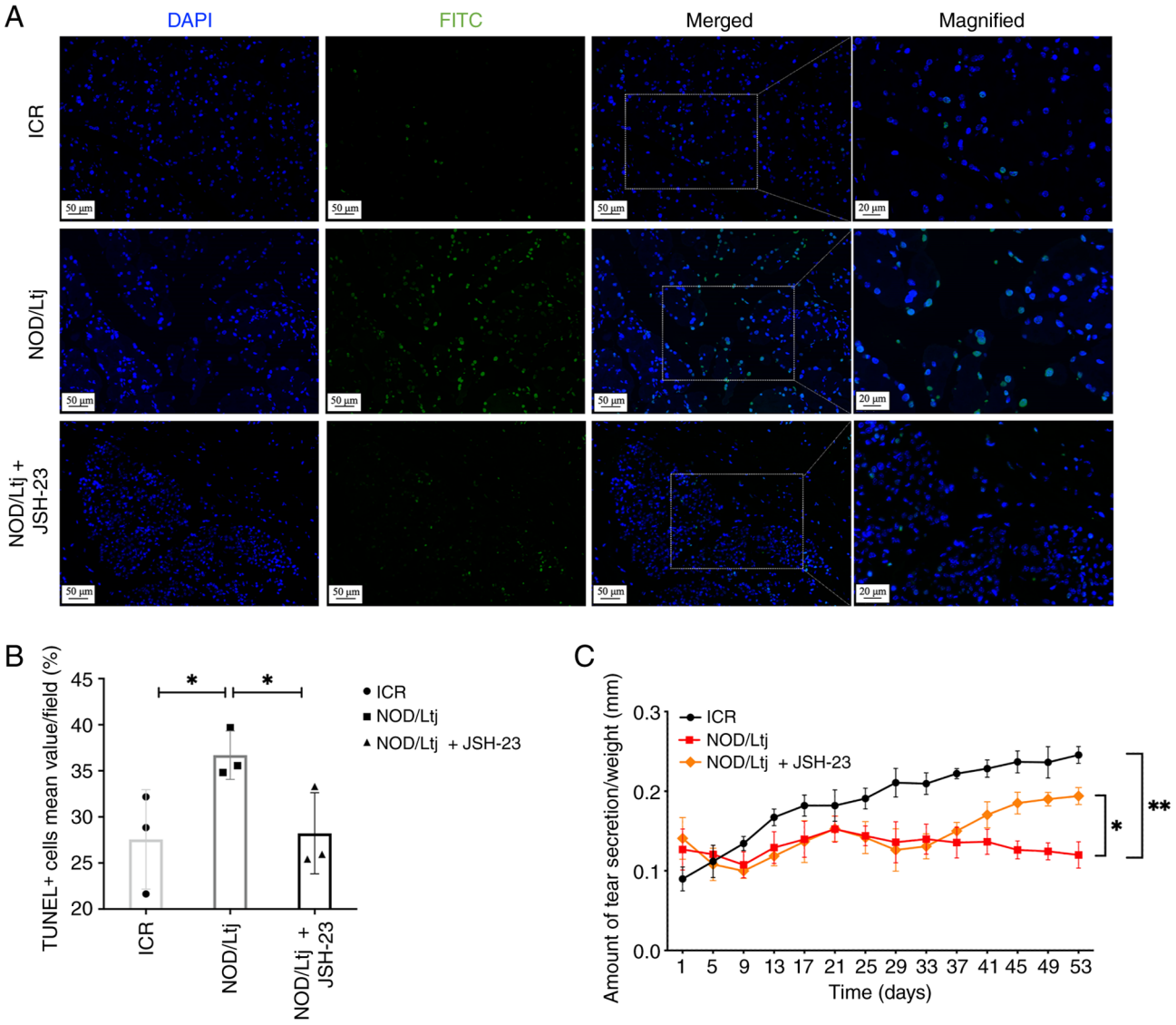

Figure 8. JSH-23 reduces lacrimal gland apoptosis and improves tear secretion in NOD/Ltj mice. (A) Representative TUNEL staining of lacrimal gland sections from ICR, NOD/Ltj and NOD/Ltj + JSH-23 groups (scale bars, 50 and 20 μm). (B) Quantitative analysis of apoptotic cells expressed as percentage (%) of TUNEL$^+$ cells compared with total DAPI-stained nuclei. (C) Tear secretion measured by the phenol red thread assay. Data are presented as mean ± SD (n=4 per group). *P<0.05 and **P<0.01 vs. NOD/Ltj group; ns, not significant vs. ICR control. SD, standard deviation; NOD, non-obese diabetic; ICR, Institute of Cancer Research; TUNEL, terminal deoxynucleotidyl transferase dUTP nick end labeling; DAPI, 4',6-diamidino-2-phenylindole.

dysfunction (50,51,53). Therapeutic targeting of NF-κB has been proposed as a strategy to attenuate glandular inflammation while preserving epithelial integrity (54). Modulation of NF-κB pathway components, including IKKε and IκBα, as well as associations with anti-SS-related antigen A autoantibodies, have been reported in pSS (55,56). Small-molecule inhibitors with NF-κB-modulatory properties, such as iguratimod, have advanced to clinical evaluation (54). Clinical studies indicated that iguratimod, when combined with hydroxychloroquine and glucocorticoids, improves xerostomia and xerophthalmia, reduces disease activity and does not increase adverse events, including gastrointestinal symptoms, liver function abnormalities and leukopenia (57-59). By contrast, other targeted therapies, such as the spleen tyrosine kinase inhibitor GS-9876, have not demonstrated notable clinical benefit in pSS (60). Although these clinical findings supported the therapeutic potential of NF-κB modulation, the protective mechanisms operating within the lacrimal gland remain incompletely defined.

Dry eye in pSS is a marked lack of aqueous tears caused by lacrimal gland destruction. During the experimental design phase, the potential use of JSH-23 as a topical eye drop was carefully evaluated. Previous studies have demonstrated that targeting the NF-κB pathway effectively mitigates ocular surface inflammation (61-63). However, those interventions primarily target ocular surface epithelia. Anatomically, the lacrimal gland is an extraocular exocrine gland located deep within the orbit, producing aqueous tears that flow directionally onto the ocular surface via excretory ducts. Due to this directional fluid flow and deep anatomical location, topically applied eye drops possess a limited ability to penetrate retrogradely to reach the glandular microenvironment. Therefore, a topical formulation would not effectively treat the primary glandular lesions characteristic of pSS. Therefore, systemic

administration was selected to address the underlying etiology. Unlike intraocular tissues protected by the blood ocular barrier, the extraocular lacrimal gland is highly vascularized in the orbit. Systemic oral administration utilizes the bloodstream to deliver the therapeutic agent directly into this target tissue. Although precise ocular bioavailability and absolute local drug concentrations were not directly quantified via pharmacokinetic measurements in the present study, pharmacological inhibition of NF-κB using JSH-23 suppressed pathway activation in the lacrimal glands and was associated with reduced systemic levels of IFN-γ, TNF-α and IL-17A. Previous studies suggested that glandular epithelial cells may serve as initiators of inflammatory cascades in pSS, contributing to a self-perpetuating cycle of tissue injury and immune activation (64-66). NF-κB signaling has been implicated in epithelial apoptosis and inflammatory amplification (51). Consistent with this framework, the present study demonstrated that JSH-23 treatment reduced lacrimal gland apoptosis and partially restored tear secretion. This restoration aligns with the recovered expression level of CARD14, suggesting that attenuation of NF-κB mediated inflammation may contribute to improved epithelial survival and glandular function by disrupting the local inflammatory vicious cycle.

In addition to tear volume, the biochemical composition of tears serves a key role in ocular surface health. The lacrimal gland secretes the aqueous layer of the tear film containing functional proteins such as lactoferrin and lysozyme, while mucins are primarily produced by the ocular surface epithelium (67). In pSS, autoimmune destruction of the lacrimal gland leads to deficiency in these protective proteins. These alterations directly disrupt the ocular surface microenvironment and compromise tear film stability. Despite the high clinical relevance of these changes, the severe aqueous deficiency in the NOD Ltj mouse model precluded the collection of sufficient tear fluid for reliable quantitative analysis in the present study. Future research utilizing specialized microvolume proteomic technologies are warranted to comprehensively evaluate these compositional changes and identify potential biomarkers (68).

Th17 cells represent a key effector subset in pSS-associated target organ damage. Increased Th17 cell infiltration has been documented in salivary glands of patients with pSS and has been associated with disease severity (69,70). As the signature cytokine of Th17 cells, IL-17A amplifies inflammatory cascades by promoting the production of additional pro-inflammatory mediators, including TNF-α (71,72). While experimental studies in pSS models further support a pathogenic role for Th17 cells during early glandular inflammation (70,73,74), the specific molecular pathways that govern their recruitment to the lacrimal gland remain less defined compared with those in the salivary glands. In the present study model, NOD/Ltj mice exhibited increased systemic and local Th17 cell frequency, accompanied by elevated IL-17A expression in lacrimal glands. NF-κB signaling has been reported to regulate transcription factors such as retinoic acid receptor-related orphan receptor-γt and to facilitate IL-17A production, thereby promoting Th17 cell differentiation and sustained inflammatory responses in pSS (54). Inhibition of NF-κB with JSH-23 significantly reduced both systemic Th17 cell frequency and local $CD4^+IL\text{-}17A^+$ cell infiltration into the lacrimal gland. These findings supported a mechanistic association between NF-κB activation and Th17-driven inflammation in pSS lacrimal gland pathology.

The present study defined the transcriptomic signatures specific to the lacrimal gland microenvironment. First, to the best of our knowledge, the present study identified *CARD14* as a newly reported DEG in pSS lacrimal tissues. The marked downregulation of *CARD14* in the disease model of the present study indicated a distinct function in maintaining glandular epithelial integrity. Second, by applying high-throughput mRNA-seq, a localized regulatory network was mapped that associated *CARD14* dysregulation and NF-κB activation with subsequent chemokine such as CCL19 release and Th17 recruitment. Third, *in vivo* experiments also demonstrated that targeted NF-κB inhibition with JSH-23 not only slows disease progression but directly restores local glandular secretory function and promotes epithelial survival.

Several limitations need to be acknowledged in the present study. First, the sample size utilized for the RNA sequencing analysis was relatively small which may limit the overall statistical power to capture all transcriptomic alterations. Second, the *in vivo* intervention employed a single dose of JSH-23 and longitudinal progression of lacrimal gland pathology was not systematically evaluated. Therefore, the dose-response relationship and long-term pharmacological safety of NF-κB inhibition remain to be elucidated in future research. Third, although the present study findings demonstrated decreased Th17 cell frequency following pathway inhibition, the precise molecular mechanisms that associate NF-κB activation with Th17 differentiation were not directly investigated. Specifically, directed gain/loss of function experiments are warranted to confirm the roles of CARD14 and CCL19. Future longitudinal studies incorporating optimized sample collection strategies are warranted to clarify the long-term impact of NF-κB inhibition and comprehensively evaluate these compositional changes. Furthermore, integrating these experimental findings with emerging artificial intelligence tools in medical informatics may hold notable potential in translating preclinical findings into precision therapies for patients with pSS (75).

In summary, the present study demonstrated that CARD14 dysregulation and the subsequent hyperactivation of the NF-κB signaling pathway contributes to lacrimal gland injury in a murine model of pSS. NF-κB activation was associated with enhanced Th17 cell infiltration, increased pro-inflammatory cytokine production and epithelial apoptosis, resulting in impaired tear secretion. Pharmacological inhibition of NF-κB with JSH-23 attenuated systemic and local inflammatory responses, reduced glandular apoptosis and partially restored tear secretion. Although further studies are warranted to optimize dosing strategies and define long-term safety, these findings provided *in vivo* evidence supporting NF-κB signaling as a potential therapeutic target in pSS-associated severe dry eye.

Acknowledgements

The authors would like to thank Dr Changjun Wang and Dr Yiming Sun (Eye Center of Second Affiliated Hospital, Zhejiang University School of Medicine, Zhejiang, China) for their assistance with statistical advice.

Funding

The present study was supported by funds from National Natural Science Foundation of China (grant nos. 82000938 and 82330032) and Zhejiang Provincial Key Research and Development Program (grant no. 2024C03204).

Availability of data and materials

The data generated in the present study may be found in the National Center for Biotechnology Information (NCBI) Gene Expression Omnibus repository under the accession number GSE306385 or at the following URL: https://www.ncbi.nlm.nih.gov/geo/query/acc.cgi?acc=GSE306385. The corresponding raw mRNA-seq data generated in the present study may be found in the NCBI Sequence Read Archive under the BioProject accession number PRJNA1310557 or at the following URL: https://www.ncbi.nlm.nih.gov/Traces/study/?acc=PRJNA1310557&o=acc_s%3Aa.

Authors' contributions

JX conceptualized the present study, devised the methodology, conducted the investigation, acquired funding and wrote the original draft. HZ devised the methodology, conducted the investigation and formal analysis, and wrote the original draft. WS devised the methodology, conducted the investigation and formal analysis. JY conceptualized the present study, provided supervision, acquired funding, obtained resources, participated in project administration, reviewed and edited the manuscript. JX and JY confirm the authenticity of all the raw data. All authors read and approved the final manuscript.

Ethics approval and consent to participate

All animal experiments were approved by the Animal Ethics Committee of the Second Affiliated Hospital of Zhejiang University School of Medicine (approval no. 2022 NO.190; Zhejiang, China).

Patient consent for publication

Not applicable.

Competing interests

The authors declare that they have no competing interests.

References

1. Bjordal O, Norheim KB, Rødahl E, Jonsson R and Omdal R: Primary Sjögren's syndrome and the eye. Surv Ophthalmol 65: 119-132, 2020.
2. Xu D, Zhao S, Li Q, Wang YH, Zhao JL, Li MT, Zhao Y and Zeng XF: Characteristics of Chinese patients with primary Sjögren's syndrome: Preliminary report of a multi-centre registration study. Lupus 29: 45-51, 2020.
3. Bron AJ, de Paiva CS, Chauhan SK, Bonini S, Gabison EE, Jain S, Knop E, Markoulli M, Ogawa Y, Perez V, *et al*: TFOS DEWS II pathophysiology report. Ocul Surf 15: 438-510, 2017.
4. Bodewes ILA, Björk A, Versnel MA and Wahren-Herlenius M: Innate immunity and interferons in the pathogenesis of Sjögren's syndrome. Rheumatology (Oxford) 60: 2561-2573, 2021.
5. Kwok SK, Cho ML, Her YM, Oh HJ, Park MK, Lee SY, Woo YJ, Ju JH, Park KS, Kim HY and Park SH: TLR2 ligation induces the production of IL-23/IL-17 via IL-6, STAT3 and NF-kB pathway in patients with primary Sjogren's syndrome. Arthritis Res Ther 14: R64, 2012.
6. Li P, Yang Y, Jin Y, Zhao R, Dong C, Zheng W, Zhang T, Li J and Gu Z: B7-H3 participates in human salivary gland epithelial cells apoptosis through NF-κB pathway in primary Sjögren's syndrome. J Transl Med 17: 268, 2019.
7. Zheng X, Wang Q, Yuan X, Zhou Y, Chu H, Wang G, Li X, Wang Y, Wei L, Wang L and Li X: B7-H4 inhibits the development of primary Sjögren's syndrome by regulating treg differentiation in NOD/Ltj mice. J Immunol Res 2020: 4896727, 2020.
8. Zheng Q, Ren Y, Reinach PS, She Y, Xiao B, Hua S, Qu J and Chen W: Reactive oxygen species activated NLRP3 inflammasomes prime environment-induced murine dry eye. Exp Eye Res 125: 1-8, 2014.
9. Mariette X and Criswell LA: Primary Sjögren's syndrome. N Engl J Med 378: 931-939, 2018.
10. Brito-Zerón P, Baldini C, Bootsma H, Bowman SJ, Jonsson R, Mariette X, Sivils K, Theander E, Tzioufas A and Ramos-Casals M: Sjögren syndrome. Nat Rev Dis Primers 2: 16047, 2016.
11. Ogawa Y, Shimizu E and Tsubota K: Interferons and dry eye in Sjögren's syndrome. Int J Mol Sci 19: 3548, 2018.
12. Liao J, Yu X, Huang Z, He Q, Yang J, Zhang Y, Chen J, Song W, Luo J and Tao Q: Chemokines and lymphocyte homing in Sjögren's syndrome. Front Immunol 15: 1345381, 2024.
13. Fu L, Zhao Z, Zhao S, Zhang M, Teng X, Wang L and Yang T: The involvement of aquaporin 5 in the inflammatory response of primary Sjogren's syndrome dry eye: Potential therapeutic targets exploration. Front Med (Lausanne) 11: 1439888, 2024.
14. Gao M, Zhao L, Liang R, Zhu Q, Zhao Q and Kong X: Evaluation of the efficacy and safety of topical 0.05% cyclosporine eye drops (II) in the treatment of dry eye associated with primary Sjögren's syndrome. Ocul Immunol Inflamm 31: 1662-1668, 2023.
15. Gao Y, Chen Y, Zhang Z, Yu X and Zheng J: Recent advances in mouse models of Sjögren's syndrome. Front Immunol 11: 1158, 2020.
16. Park YS, Gauna AE and Cha S: Mouse models of primary Sjogren's syndrome. Curr Pharm Des 21: 2350-2364, 2015.
17. Humphreys-Beher MG, Hu Y, Nakagawa Y, Wang PL and Purushotham KR: Utilization of the non-obese diabetic (NOD) mouse as an animal model for the study of secondary Sjögren's syndrome. In: Lacrimal Gland, Tear Film, and Dry Eye Syndromes: Basic Science and Clinical Relevance. Springer US, Boston, MA, pp631-636, 1994.
18. Kumar A, Negi G and Sharma SS: JSH-23 targets nuclear factor-kappa B and reverses various deficits in experimental diabetic neuropathy: Effect on neuroinflammation and antioxidant defence. Diabetes Obes Metab 13: 750-758, 2011.
19. Nassar A, Kaplanski J and Azab AN: A selective nuclear factor-κB inhibitor, JSH-23, exhibits antidepressant-like effects and reduces brain inflammation in rats. Pharmaceuticals (Basel) 17: 1271, 2024.
20. Percie du Sert N, Hurst V, Ahluwalia A, Alam S, Avey MT, Baker M, Browne WJ, Clark A, Cuthill IC, Dirnagl U, *et al*: The ARRIVE guidelines 2.0: Updated guidelines for reporting animal research. PLoS Biol 18: e3000410, 2020.
21. National Research Council: Committee for the Update of the Guide for the Care and Use of Laboratory Animals: Guide for the care and use of laboratory animals. 8th edition. National Academies Press US, Washington, DC, 2011.
22. Livak KJ and Schmittgen TD: Analysis of relative gene expression data using real-time quantitative PCR and the 2(-Delta Delta C(T)) method. Methods 25: 402-408, 2001.
23. Singh S, Jasani G, Basu S and Varma DR: Radiological imaging of the lacrimal gland in Sjogren's syndrome: A systematic review and meta-analysis. Curr Eye Res 49: 1115-1122, 2024.
24. Shiboski CH, Shiboski SC, Seror R, Criswell LA, Labetoulle M, Lietman TM, Rasmussen A, Scofield H, Vitali C, Bowman SJ, *et al*: 2016 American college of rheumatology/European league against rheumatism classification criteria for primary Sjögren's syndrome: A consensus and data-driven methodology involving three international patient cohorts. Ann Rheum Dis 76: 9-16, 2017.
25. Daniels TE, Cox D, Shiboski CH, Schiødt M, Wu A, Lanfranchi H, Umehara H, Zhao Y, Challacombe S, Lam MY, *et al*: Associations between salivary gland histopathologic diagnoses and phenotypic features of Sjögren's syndrome among 1,726 registry participants. Arthritis Rheum 63: 2021-2030, 2011.

26. Gottenberg JE, Cagnard N, Lucchesi C, Letourneur F, Mistou S, Lazure T, Jacques S, Ba N, Ittah M, Lepajolec C, *et al*: Activation of IFN pathways and plasmacytoid dendritic cell recruitment in target organs of primary Sjögren's syndrome. Proc Natl Acad Sci USA 103: 2770-2775, 2006.
27. Brkic Z and Versnel MA: Type I IFN signature in primary Sjögren's syndrome patients. Expert Rev Clin Immunol 10: 457-467, 2014.
28. Chen C, Liang Y, Zhang Z, Zhang Z and Yang Z: Relationships between increased circulating YKL-40, IL-6 and TNF-α levels and phenotypes and disease activity of primary Sjögren's syndrome. Int Immunopharmacol 88: 106878, 2020.
29. Zhang L, Xu P, Wang X, Zhang Z, Zhao W, Li Z, Yang G and Liu P: Identification of differentially expressed genes in primary Sjögren's syndrome. J Cell Biochem 120: 17368-17377, 2019.
30. Li N, Li L, Wu M, Li Y, Yang J, Wu Y, Xu H, Luo D, Gao Y, Fei X and Jiang L: Integrated bioinformatics and validation reveal potential biomarkers associated with progression of primary Sjögren's syndrome. Front Immunol 12: 697157, 2021.
31. Lin Y, Yao X, Yan M, Zhou L, Huang W, Xiao Y, Wu D and Chen J: Integrated analysis of transcriptomics to identify hub genes in primary Sjögren's syndrome. Oral Dis 28: 1831-1845, 2022.
32. Vitali C, Dolcino M, Del Papa N, Minniti A, Pignataro F, Maglione W, Lunardi C and Puccetti A: Gene expression profiles in primary Sjögren's syndrome with and without systemic manifestations. ACR Open Rheumatol 1: 603-613, 2019.
33. Cui J, Li H, Wang T, Shen Q, Yang Y, Yu X and Hu H: Novel Immune-related genetic expression for primary Sjögren's syndrome. Front Med (Lausanne) 8: 719958, 2022.
34. Mauduit O, Delcroix V, Umazume T, de Paiva CS, Dartt DA and Makarenkova HP: Spatial transcriptomics of the lacrimal gland features macrophage activity and epithelium metabolism as key alterations during chronic inflammation. Front Immunol 13: 1011125, 2022.
35. Rattner A, Heng JS, Winer BL, Goff LA and Nathans J: Normal and Sjogren's syndrome models of the murine lacrimal gland studied at single-cell resolution. Proc Natl Acad Sci USA 120: e2311983120, 2023.
36. Nguyen CQ, Sharma A, She JX, McIndoe RA and Peck AB: Differential gene expressions in the lacrimal gland during development and onset of keratoconjunctivitis sicca in Sjögren's syndrome (SJS)-like disease of the C57BL/6.NOD-Aec1Aec2 mouse. Exp Eye Res 88: 398-409, 2009.
37. Israel L and Mellett M: Clinical and genetic heterogeneity of CARD14 mutations in psoriatic skin disease. Front Immunol 9: 2239, 2018.
38. Ikawa T, Ichimura Y, Miyagawa T, Fukui Y, Toyama S, Omatsu J, Awaji K, Norimatsu Y, Watanabe Y, Yoshizaki A, *et al*: The contribution of LIGHT (TNFSF14) to the development of systemic sclerosis by modulating IL-6 and T helper type 1 chemokine expression in dermal fibroblasts. J Invest Dermatol 142: 1541-1551.e3, 2022.
39. Han M, Sun Y, Zhao W, Xiang G, Wang X, Jiang Z, Xue Z and Zhou W: Comprehensive characterization of TNFSF14/LIGHT with implications in prognosis and immunotherapy of human gliomas. Front Immunol 13: 1025286, 2022.
40. Chen R, Wang X, Dai Z, Wang Z, Wu W, Hu Z, Zhang X, Liu Z, Zhang H and Cheng Q: TNFSF13 is a novel onco-inflammatory marker and correlates with immune infiltration in gliomas. Front Immunol 12: 713757, 2021.
41. Yu Q, Lou XM and He Y: Preferential recruitment of Th17 cells to cervical cancer via CCR6-CCL20 pathway. PLoS One 10: e0120855, 2015.
42. Hauser MA and Legler DF: Common and biased signaling pathways of the chemokine receptor CCR7 elicited by its ligands CCL19 and CCL21 in leukocytes. J Leukoc Biol 99: 869-882, 2016.
43. Yang J, Agarwal M, Ling S, Teitz-Tennenbaum S, Zemans RL, Osterholzer JJ, Sisson TH and Kim KK: Diverse injury pathways induce alveolar epithelial Cell CCL2/12, which promotes lung fibrosis. Am J Respir Cell Mol Biol 62: 622-632, 2020.
44. Scudiero I, Zotti T, Ferravante A, Vessichelli M, Vito P and Stilo R: Alternative splicing of CARMA2/CARD14 transcripts generates protein variants with differential effect on NF-κB activation and endoplasmic reticulum stress-induced cell death. J Cell Physiol 226: 3121-3131, 2011.
45. Bertin J, Wang L, Guo Y, Jacobson MD, Poyet JL, Srinivasula SM, Merriam S, DiStefano PS and Alnemri ES: CARD11 and CARD14 are novel caspase recruitment domain (CARD)/membrane-associated guanylate kinase (MAGUK) family members that interact with BCL10 and activate NF-kappa B. J Biol Chem 276: 11877-11882, 2001.
46. Howes A, O'Sullivan PA, Breyer F, Ghose A, Cao L, Krappmann D, Bowcock AM and Ley SC: Psoriasis mutations disrupt CARD14 autoinhibition promoting BCL10-MALT1-dependent NF-κB activation. Biochem J 473: 1759-1768, 2016.
47. Liu Z, Li F, Pan A, Xue H, Jiang S, Zhu C, Jin M, Fang J, Zhu X, Brown MA and Wang X: Elevated CCL19/CCR7 expression during the disease process of primary Sjögren's syndrome. Front Immunol 10: 795, 2019.
48. Yu HR, Sung ML, Kuo HC, Lin CH and Chen CN: Shear stress modulates resistin-induced CC chemokine ligand 19 expression in human aortic endothelial cells. J Cell Physiol 230: 2120-2127, 2015.
49. Pisani LF, Tontini G, Vecchi M, Croci GA and Pastorelli L: NF-kB pathway is involved in microscopic colitis pathogenesis. J Int Med Res 50: 03000605221080104, 2022.
50. Sisto M, Ribatti D and Lisi S: Understanding the complexity of Sjögren's syndrome: Remarkable progress in elucidating NF-κB mechanisms. J Clin Med 9: 2821, 2020.
51. Wang X, Shaalan A, Liefers S, Coudenys J, Elewaut D, Proctor GB, Bootsma H, Kroese FGM and Pringle S: Dysregulation of NF-kB in glandular epithelial cells results in Sjögren's-like features. PLoS One 13: e0200212, 2018.
52. Lisi S, Sisto M, Lofrumento DD and D'Amore M: Sjögren's syndrome autoantibodies provoke changes in gene expression profiles of inflammatory cytokines triggering a pathway involving TACE/NF-κB. Lab Invest 92: 615-624, 2012.
53. Shimizu T, Nakamura H and Kawakami A: Role of the innate immunity signaling pathway in the pathogenesis of Sjögren's syndrome. Int J Mol Sci 22: 3090, 2021.
54. Pringle S, Wang X, Bootsma H, Spijkervet FKL, Vissink A and Kroese FGM: Small-molecule inhibitors and the salivary gland epithelium in Sjögren's syndrome. Expert Opin Investig Drugs 28: 605-616, 2019.
55. Chen W, Lin J, Cao H, Xu D, Xu B, Xu L, Yue L, Sun C, Wu G and Qian W: Local and systemic IKKε and NF-κB signaling associated with Sjögren's syndrome immunopathogenesis. J Immunol Res 2015: 534648, 2015.
56. Sisto M, Lisi S, Lofrumento DD, Ingravallo G, De Lucro R and D'Amore M: Salivary gland expression level of IκBα regulatory protein in Sjögren's syndrome. J Mol Histol 44: 447-454, 2013.
57. Pu J, Wang X, Riaz F, Zhang T, Gao R, Pan S, Wu Z, Liang Y, Zhuang S and Tang J: Effectiveness and safety of iguratimod in treating primary Sjögren's Syndrome: A systematic review and meta-analysis. Front Pharmacol 12: 621208, 2021.
58. Zeng L, He Q, Yang K, Hao W, Yu G and Chen H: A systematic review and meta-analysis of 19 randomized controlled trials of iguratimod combined with other therapies for Sjögren's syndrome. Front Immunol 13: 924730, 2022.
59. Long Z, Zeng L, He Q, Yang K, Xiang W, Ren X, Deng Y and Chen H: Research progress on the clinical application and mechanism of iguratimod in the treatment of autoimmune diseases and rheumatic diseases. Front Immunol 14: 1150661, 2023.
60. Wang B, Chen S, Li Y, Xuan J, Liu Y and Shi G: Targeted therapy for primary Sjögren's syndrome: Where are we now? BioDrugs 35: 593-610, 2021.
61. Zhang X, Yin Y, Yue L and Gong L: Selective serotonin reuptake inhibitors aggravate depression-associated dry eye via activating the NF-κB pathway. Invest Ophthalmol Vis Sci 60: 407-419, 2019.
62. Yu Z, Yazdanpanah G, Alam J, de Paiva CS and Pflugfelder S: Induction of innate inflammatory pathways in the corneal epithelium in the desiccating stress dry eye model. Invest Ophthalmol Vis Sci 64: 8, 2023.
63. Zhou Y, Ma B, Liu Q, Duan H, Huo Y, Zhao L, Chen J, Han W and Qi H: Transmembrane protein CMTM6 alleviates ocular inflammatory response and improves corneal epithelial barrier function in experimental dry eye. Invest Ophthalmol Vis Sci 65: 4, 2024.
64. Katsiougiannis S, Tenta R and Skopouli FN: Autoimmune epithelitis (Sjögren's syndrome); the impact of metabolic status of glandular epithelial cells on auto-immunogenicity. J Autoimmun 104: 102335, 2019.
65. Moutsopoulos HM: Sjögren's syndrome: Autoimmune epithelitis. Clin Immunol Immunopathol 72: 162-165, 1994.

66. Manoussakis MN and Kapsogeorgou EK: The role of intrinsic epithelial activation in the pathogenesis of Sjögren's syndrome. J Autoimmun 35: 219-224, 2010.
67. Versura P, Bavelloni A, Grillini M, Fresina M and Campos EC: Diagnostic performance of a tear protein panel in early dry eye. Mol Vis 19: 1247-1257, 2013.
68. Das N, Menon NG, de Almeida LGN, Woods PS, Heynen ML, Jay GD, Caffery B, Jones L, Krawetz R, Schmidt TA and Dufour A: Proteomics analysis of tears and saliva from Sjogren's syndrome patients. Front Pharmacol 12: 787193, 2021.
69. Voigt A, Bohn K, Sukumaran S, Stewart CM, Bhattacharya I and Nguyen CQ: Unique glandular ex-vivo Th1 and Th17 receptor motifs in Sjögren's syndrome patients using single-cell analysis. Clin Immunol 192: 58-67, 2018.
70. Verstappen GM, Corneth OBJ, Bootsma H and Kroese FGM: Th17 cells in primary Sjögren's syndrome: Pathogenicity and plasticity. J Autoimmun 87: 16-25, 2018.
71. Veldhoen M: Interleukin 17 is a chief orchestrator of immunity. Nat Immunol 18: 612-621, 2017.
72. Fei Y, Zhang W, Lin D, Wu C, Li M, Zhao Y, Zeng X and Zhang F: Clinical parameter and Th17 related to lymphocytes infiltrating degree of labial salivary gland in primary Sjögren's syndrome. Clin Rheumatol 33: 523-529, 2014.
73. Nguyen CQ, Yin H, Lee BH, Carcamo WC, Chiorini JA and Peck AB: Pathogenic effect of interleukin-17A in induction of Sjögren's syndrome-like disease using adenovirus-mediated gene transfer. Arthritis Res Ther 12: R220, 2010.
74. Katsifis GE, Rekka S, Moutsopoulos NM, Pillemer S and Wahl SM: Systemic and local interleukin-17 and linked cytokines associated with Sjögren's syndrome immunopathogenesis. Am J Pathol 175: 1167-1177, 2009.
75. Lin H: Artificial intelligence with great potential in medical informatics: A brief review. Medinformatics 1: 2-9, 2024.